Study of Hydrogen Recycling and Plasma Detachment by Utilizing End-loss Plasma of the GAMMA 10/PDX Tandem Mirror

Akihiro Terakado

February 2019

Study of Hydrogen Recycling and Plasma Detachment by Utilizing End-loss Plasma of the GAMMA 10/PDX Tandem Mirror

Akihiro Terakado
Doctoral Program in Physics

Submitted to the Graduate School of
Pure and Applied Sciences
in Partial Fulfillment of the Requirements
for the Degree of Doctor of Philosophy in
Science

at the
University of Tsukuba

Contents

Chapter 1 Introduction 3
1.1 Nuclear Fusion 3
1.2 Divertor 4
1.2.1 Outline of divertor 4
1.2.1 Research tasks for the divertor 5
1.3 Plasma detachment 6
1.3.1 Outline of plasma detachment 6
1.3.2 Research tasks for the plasma detachment and molecular processes 7
1.4. Introduction of studies of hydrogen recycling 9
1.5 Motivation and outline of thesis 10
Chapter 2 Atomic and molecular processes of hydrogen plasma 12
2.1 Characteristics of hydrogen atoms and molecules 12
2.1.1 Electron energy levels of atom and molecular 12
2.1.3 Fulcher-α band 17
2.1.4 Vibrational and rotational temperature of hydrogen 18
2.2 Hydrogen recycling 20
2.3 Molecular activated recombination (MAR) 22
Chapter 3 Experimental setup 25
3.1 GAMMA 10/PDX 25
3.2 Divertor simulation experimental module (D-module) 26
3.2.1 Specifications of D-module 26
3.2.2 Plasma diagnostics 28
Chapter 4 Hydrogen recycling with high temperature tungsten target 29
4.1 Experimental method 30
4.2 Experimental result and Discussion 32
4.3 Summary 37
Chapter 5 Plasma detachment caused by molecular activated recombination 38
5.1 Experimental method 38
5.2 Experimental result 38
5.2.1 Typical behavior of the main plasma 38
5.2.2 Plasma parameters of detached plasma 40
5.2.3 Spatial distribution of MAR 41
5.2.4 Observation of transition to MAR with population inversion 44
5.3 Discussion 48
5.3.1 Recombination processes of the detached plasma 48
5.3.2 MAR with highly excited Balmer emissions and population inversion 49

5.4 Summary 50
Chapter 6 Dynamic behavior of plasma detachment caused by MAR 51
6.1 Experimental method 51
6.2 Experimental result and Discussion 51
6.3 Summary 58
Chapter 7 Conclusion 59
Acknowledgements 60
References 61

Chapter 1
Introduction

1.1 Nuclear Fusion

We the humans have been expanding means of using energy and the amount of energy consumption continues to increase, from the discovery of fire which is the first acquisition of the means of using energy until today. In today's world, fossil fuels such as coal, oil and natural gas constitute more than half of energy sources [1]. Fossil fuels will be exhausted in the future and excessive consumption of it leads to environmental problems such as air pollution and global warming. In addition, the population of the world continues to increase, and it is thought that the trend of increase in energy consumption will become even bigger in the future. Therefore, it is subject that the development of substituting fossil fuels, reducing the environmental burden and addressing the increase in energy that will be needed in the future. The development of nuclear fusion reactor (i.e. nuclear fusion power generation) has been considered as the most promising solutions.

In the nuclear fusion reaction, the interaction of two or more atomic nuclei which lighter than the iron nucleus, leads to the production of different nuclei and energy. That produced energy equals to the mass difference before and after the reaction (i.e. mass defect). A nuclear fusion reaction occurs when the nuclei overcome the Coulomb repulsion force and get closer to the range where strong interaction occurs. Candidate reactions using for the fusion reactor are shown below.

$$D + D \rightarrow T + p + 4.032\ \text{MeV} \quad (1.1)$$
$$D + D \rightarrow {}^{3}He + n + 3.2\ \text{MeV} \quad (1.2)$$
$$D + T \rightarrow {}^{4}He + n + 17.586\ \text{MeV} \quad (1.3)$$
$$D + {}^{3}He \rightarrow {}^{4}He + p + 18.341\ \text{MeV} \quad (1.4)$$

The reaction of deuterium and tritium (1.3) which has the large cross section at a relatively low energy is used for the International Thermonuclear Experimental Reactor (ITER) and a prototype reactor (i.e. DEMO).

In the world, the control of nuclear fusion plasma has been studying studied for the development of thermonuclear fusion reactor. It is necessary to confine a plasma which has a temperature for more than 10 keV with a high density (i.e. achievement of Lawson criterion [2])

in order to obtain net energy from fusion plasma. Production of break-even plasma (i.e. Fusion energy gain factor Q = 1) has been achieved in JET [3] and JT-60U [4]. At present, construction of the ITER is developing for plasma production with Q = 5 ~ 10 and it is funded by 7 entities (European Union, India, Japan, China, Russia, South Korea, and the United States) [5]. In ITER, physics of break-even plasma are investigated and essential technics such as steady-state operation and high-temperature blanket are developed [6]. Furthermore, a prototype reactor (i.e. DEMO) is designed for the demonstration of the technical feasibility of nuclear fusion energy and completion of the research and development stage, by utilizing the physical and engineering knowledge obtained by ITER.

1.2 Divertor

1.2.1 Outline of divertor

In order to develop the fusion reactor, it is important to enhance plasma confinement performance. It is necessary to reduce impurities flowing into the core plasma and handle properly heat and particle flowing from the core plasma, in order to improve plasma confinement performance. In 1958 L. Spitzer suggested the concept of magnetic divertor [7], in order to broaden the heat receiving area of the plasma-facing components and to reduce the heat load to the facing components. In the tokamak device which contrasts in the toroidal direction, the

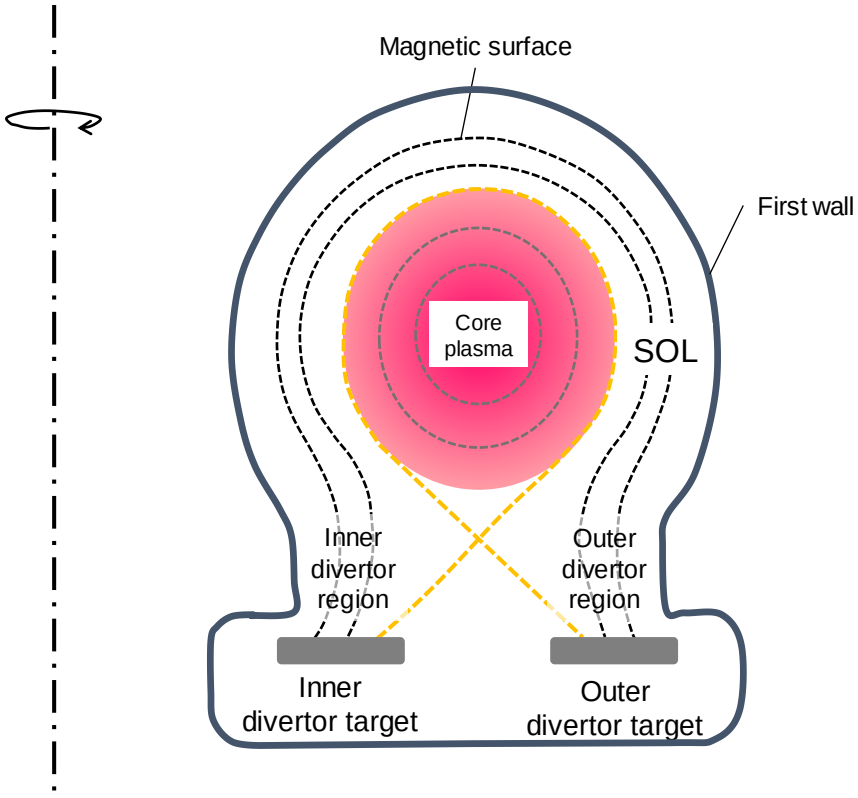

Fig.1.1 Poloidal cross-section of tokamak.

diverter configuration consists of a poloidal magnetic field which is created by a toroidal coil [8]. Figure 1.1 shows a poloidal section of the tokamak. As shown in Fig. 1.1, in the tokamak, core plasma is confined in the core region by the magnetic field. The outside of the core plasma region where magnetic field lines are in contact with the wall of the vacuum vessel (i.e. divertor plate) is called a scrape-off layer (SOL). Heat and particle fluxes flowing out from the core plasma is transported to the diverter through SOL. Since the core plasma and the vacuum vessel do not contact directly, it is possible to reduce the production of impurities from the walls and inflow of the impurities into the core plasma. In the tokamak of the divertor magnetic field configuration, it is achieved that the discharge which the energy confinement performance was significantly improved (i.e. H-mode) [9].

1.2.1 Research tasks for the divertor

The heat flow flowing out to SOL increased along with the enlargement of the device size and the improvement of the performance of the core plasma, therefore, it is serious problem that the diverter target receives a large heat load and particle flux. In ITER, it is estimated that about 100 MW of energy is released from the core plasma. Also, the width of SOL is very narrow (few mm) [10]. If no measures are taken, the divertor target will receive a heat load (i.e. Tens of MW/m2) that exceeds the heat removal performance of divertor target (i.e. ~10 MW/m2 at steady state) [11]. Therefore, it is an important task to reduce the heat load on the diverter target.

When a hydrogen ion strikes on the wall, 13.6 eV of energy corresponding to the potential energy of the hydrogen ion is released to the wall. It is not possible to reduce heat load enough by only reduce plasma temperature due to an increase in surface recombination of ions [12]. It is necessary to reduce the ion flux toward the diverter in order to reduce the heat load on the diverter target. Various studies have been made to reduce the heat load to the diverter target (e.g. detached divertor [12], radiation cooling [13], ergodic diverter [14], RF diverter [15], liquid metal divertor [16], *etc.*). Divertor detachment by the volumetric recombination is considered to be the most promising solution. Research on maintaining high recycling in divertor led to the idea of detached diverter [17]. The detached plasma is effectively produced by supplying additional gas to the divertor region. In the detached divertor plasma, ion flux rollover towards the divertor target was observed [18]. The theoretical mechanism of rollover of ion flux was explained [12, 19] and it has been experimentally investigated by the diverter of torus devices [13, 18] and the divertor simulation experiment by utilizing linear devices [21, 22].

In the H-mode plasma, the heat and particles are released from core plasma to the edge plasma at about 10-100 Hz due to MHD instability (i.e. edge localized mode (ELM)) [22]. ELMy H-mode is adopted as a standard operation mode in ITER because ELM contributes to impurity exhaust from the core plasma [23]. The divertor target at ITER transiently receives a rather

large heat load because the heat flow by ELM has 10 ~ 20% of the stored energy of the core plasma. The reaction process of the detached plasma would be transiently changed by ELM because the plasma which has two temperature distribution reaches to the diverter region by ELM [25]. In several torus devices, investigation on understanding and control of ELM are carried out [26, 27], but the influence on detached plasma has not been investigated. In linear devices, ELM has been studied only in several devices [28-31] because it is difficult to produce transient heat flow like ELM. In the detached plasma of He in NAGDIS-II, the high Rydberg atom is promptly ionized by the transient heat flow and the detached plasma becomes the attached plasma [18, 28]. In TPD-Sheet IV, the influence of pulsed plasma flow in which electrons have a high energy component has been investigated, and it has been revealed that ionization is promoted in the detached plasma by electrons with high energy components [31].

1.3 Plasma detachment

1.3.1 Outline of plasma detachment

Figure 1.2 shows the structure of detached plasma along the magnetic field line. The electron temperature decreases from the separatrix (i.e. upstream side) toward the diverter target (i.e. downstream side) and the neutral particle density increases toward the diverter plate. In the radiative region as shown in Figure 1.3, the electron temperature decreases due to the collision between neutral particles and plasmas. The electrons in the plasma lose energy by the excitation and ionization of neutrals. The momentum of the ions is reduced because the ion pressure decreases due to the collision between ions and neutral particles (i.e. elastic collision and charge exchange) [32]. In the ionization front where the electron temperature is ~ 10 eV, the electron temperature decrease and the electron density increase due to the significant increase in the ionization reaction of the neutral particles. In the recombination region, the amount of recombination reaction of the plasma exceeds the amount of ionization reaction, due to the significant decrease in electron temperature. The significant recombination reaction of plasma reduces the plasma density. Consequently, plasma pressure decreases towards diverter target and the heat flux and particle flux to the diverter target are significantly reduced. In order to produce detached plasma, it is important to increase the plasma recombination. Therefore, it is important to reveal the physics of plasma recombination.

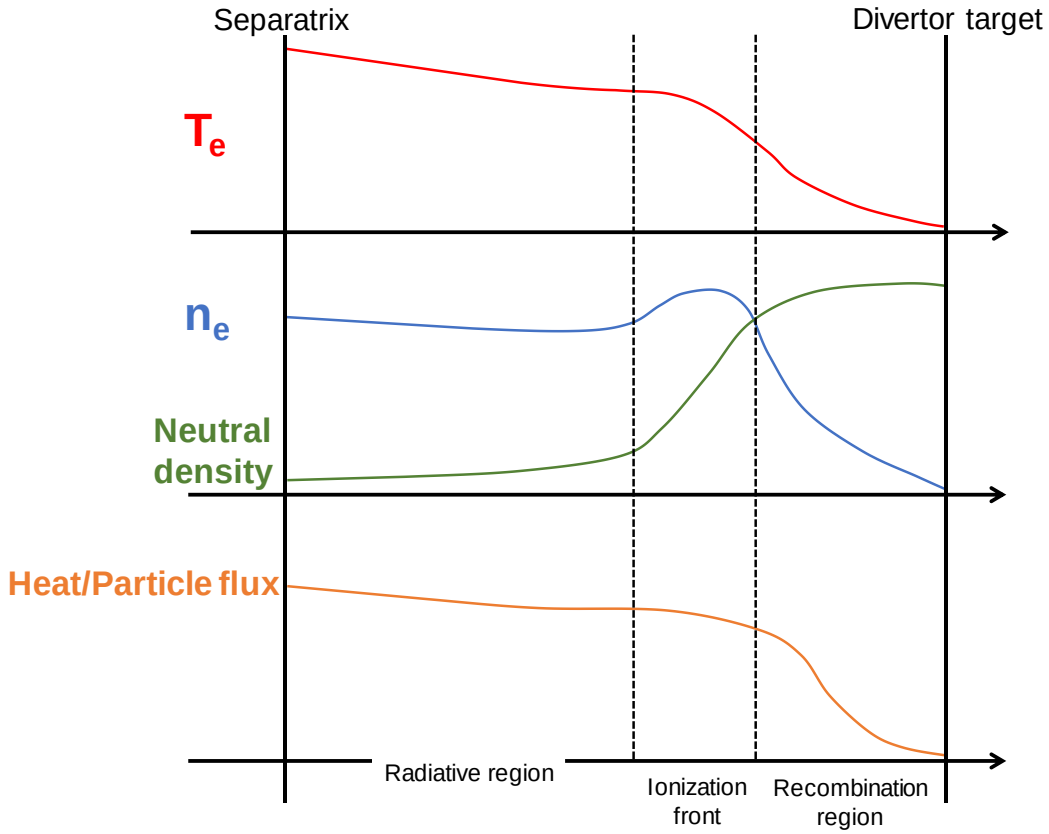

Fig.1.2 Schematic drawing of detached plasma.

1.3.2 Research tasks for the plasma detachment and molecular processes

From the viewpoint of plasma detachment, the mechanism of recombination reaction which reduces the plasma density is important. Recombination reactions in the detached plasma have been studied experimentally and theoretically [20, 21, 33-38]. In several tokamaks and linear devices, Balmer line emission from highly excited atoms has been observed in the detached plasma [39-42]. Balmer line emission from highly excited atoms in the detached plasma is caused by the EIR process (three-body recombination, radiative recombination) [36]. It is important to keep high electron density and low electron temperature in the diverter region because the rate coefficient of EIR is larger than that of ionization and the collision frequency of three-body recombination process is proportional to the cube of the electron density [36]. In the production of detached plasma, the reaction rate coefficient of EIR is quite smaller than ionization at electron temperature less than 1 eV [36]. Consequently, it is necessary to investigate the possibility of the plasma recombination mechanism at a relatively high temperature in divertor plasma detachment.

Meanwhile, Molecular activated recombination (MAR) have been studied theoretically and experimentally [35, 43, 44]. MAR is important for the production of recombining plasma because

the rate coefficient of MAR is larger than that of ionization in the relatively high electron temperature (i.e. ~ 3 eV) [43]. The reaction process of MAR is shown below.

$$H_2(v) + H^+ \rightarrow H_2^+ + H \quad (1.5)$$
$$H_2^+ + e \rightarrow H + H(n \geq 2) \quad (1.6)$$

$$H_2(v) + e \rightarrow H^- + H \quad (1.7)$$
$$H^- + H^+ \rightarrow H + H(n=2,3) \quad (1.8)$$

Reactions between vibrationally excited hydrogen molecules and plasma charged particles lead to the production of molecular ion (H_2^+) and negative ion (H^-). As shown below, there is a reaction which is a competitive reaction of MAR.

$$H_2^+ + e \rightarrow H + H^+ \quad (1.9)$$
$$H_2^+ + e \rightarrow 2H^+ \quad (1.10)$$
$$H_2(v) + e \rightarrow H^+ + H^- \quad (1.11)$$
$$H^- + e \rightarrow H^* + 2e \quad (1.12)$$

The net recombination effect by MAR is the result of competition between the reaction of (1.6) and reactions of (1.9, 1.10), the reaction of (1.7) and the reactions of (1.11), and the reaction of (1.8) and the reactions of (1.12). It is necessary to investigate the dominance of each reactions in various plasma conditions in order to clarify the net recombination effect by MAR. It has been investigated that the effective reaction rate coefficient of MAR is maximum at electron temperature is ~ 2 eV in the theoretical study and experimental study in the linear devices [43, 45]. In the Ref [43], it is reported that the reaction of (1.5) and (1.6) are most effective under the usual divertor conditions. In the TPD Sheet-IV, it is revealed that reactions of (1.7) and (1.8) are important by measurement of H^- and electron density and electron temperature in the radial profiles [46]. The measurement of molecular ions (e.g. H^-, H^+ H_2^+, H_3^+) in hydrogen plasma using an omegatron type mass spectrometer in PICSES-A, it was cleared that MAR process involving H_3^+ ions as shown below is important in the high neutral gas pressures [47].

$$H_2(v) + H_2^+ \rightarrow H_3^+ + H \quad (1.13)$$
$$H_3^+ + e \rightarrow H_2(v) + H,\ 3H \quad (1.14)$$

MAR has been observed in several diverter simulation experiments of linear devices, but it has not been observed except Alcator C-Mod, in the divertor of tokamak [48]. The reason that MAR has not been observed in tokamaks is considered to be that reactions of (1.9-1.12) become

dominant [49]. As described above, the behavior of MAR (e.g. ratio of the density of each ion species) in detached plasma is not the same in each plasma conditions of several devices. The reasons for above mentioned are considered to be that the spatial distribution of neutral gas and neutral particles with internal energy, and the behavior of plasma with their interaction. In order to investigate the possibility of MAR in diverter detachment, it is necessary for a unified understanding of atomic and molecular processes of MAR and behavior of hydrogen in the plasma-gas interaction. It is important to measure the vibrationally excited level of hydrogen molecules and to investigate the production processes of vibrationally excited molecules because the rate coefficient of MAR largely depends on the vibrationally excited level of the hydrogen molecule [45, 43].

On the other hand, in the astrophysics and process plasma for industrial applications, there is an interest in the behavior of various hydrogen ion species (e.g. ions, molecular ions, negative ions), hydrogen molecules, hydrogen atoms in the plasma-gas interactions. The main component of an atmosphere of the giant planet with large gravity (e.g. Jupiter, Saturn) is hydrogen. The behavior of low energy electrons (a few eV) and hydrogen is considered to be important to understand the composition of the upper atmosphere in the gaseous planets and the process of planet formation [50]. In addition, hydrogen plasma is used in process plasma, and it is important to understand the behavior of excited atoms, molecules and radicals for microfabrication and production of functional thin films [51]. For these reasons, researches for atomic and molecular processes of MAR has profound significance as a good ripple effects in other study fields such as astrophysics and process plasma.

1.4. Introduction of studies of hydrogen recycling

In the torus devices, the edge plasma is influenced by particle supply associated with hydrogen recycling at the first wall. Particle control in edge plasma in the long-term discharge is important for the long-term discharge because the change in the time constant of hydrogen recycling is quite long.

Recycling neutrals are atoms and molecules. The mean free path for ionization of the recycling neutrals as atom largely depends on that excited state. The mean free path for dissociation to atoms of the recycling molecules largely depends on its internal energy (e.g. vibrational excitation and rotational excitation). Dissociated atoms obtain the kinetic energy as the Franck-Condon energy of ~ 3 eV when a molecule dissociates into atoms due to electron collision. The vibrational excited state of molecules affects distribution on Frank-Condon energy. Vibrationally excited molecules are easy to dissociate to excited atoms and Frank-Condon energy which atoms are obtained is much small. The internal energy of molecules largely affects

the mean free path of ionization. Consequently, the state of the recycling particles largely affects the spatial distribution of neutrals in the edge plasma.

In some torus devices, it is observed that passively particle exhaust which particles are stored in the wall [52-54]. The amount of wall pumping decreased with the increase in plasma discharge time. That is, the global wall saturation occurred. When global wall saturation occurs, hydrogen particles are emitted from the plasma-facing wall and which makes particle control in edge plasma and control of particle balance difficult [55-60]. Particle emission due to global wall saturation correlates with the temperature of the plasma-facing walls [57, 58]. It is considered that hydrogen particles were released as molecular when the global wall saturation since the particle emission rate was changed by the change in the temperature of plasma-facing walls at several hundred degrees. It is reported that desorbed molecules are in vibrationally excited state by hot-tom recombination [61], when the particle flux to the wall is relatively large. The influence of hot-atom recombination cannot be ignored in the diverter region of tokamaks in which divertor flux is significantly high. Therefore, it is important to reveal the state of desorbed hydrogen molecules from the plasma-facing wall, in order to understand the physics of phenomenon in the edge plasma of existing devices and to estimate the density distribution of the edge plasma for future devices (e.g. DEMO).

1.5 Motivation and outline of thesis

It is difficult way to conduct fundamental research of the edge plasma (i.e. detailed parameter scan) by using a torus machine since its complex geometry make measurement difficult. In the world, elementary studies of the physics in edge plasma has been carried out utilizing linear devices. The phenomena of divertor plasma (e.g. plasma detachment) have been studied by utilizing linear devices. It is important that the phenomena of divertor plasma are studied by utilizing the plasma similar to SOL plasma in tokamaks. Ion flux comparable to SOL plasma in tokamaks has been producing in the many linear devices and the diverter simulation experiments have been conducted using them. However, there are few linear devices for divertor simulation experiment which can produce a plasma with ion temperature (~ 100 eV) comparable to SOL plasma.

GAMMA 10/PDX is the world's largest tandem mirror plasma confinement device. In GAMMA 10/PDX, divertor simulation experiments have been conducted by utilizing end-loss plasma with ion temperature close to the SOL plasma ($T_{i||}$ ~ 100 eV) [62]. The significance of utilizing GAMMA 10 / PDX for fundamental research of hydrogen recycling and plasma detachment is as follows. In GAMMA 10/PDX, the state of recycling hydrogen can be observed easily because the background neutral pressure is rather low. In addition, it is possible to control

the surface temperature of the V-shaped target which is used as the plasma-facing wall for the end loss plasma. GAMMA 10 / PDX can be utilized to investigate hydrogen recycling. GAMMA 10 / PDX has effective tools for producing, heating and maintaining the main plasma [62]. The main plasma can be stably produced even if the neutral gas pressure in the divertor experimental region is quite high. In the other words, the diverter simulation experimental region in GAMMA 10 / PDX can be operated in the wide range of plasma parameter. GAMMA 10/PDX can be utilized to investigate MAR which is useful for plasma detachment and very interesting in academically.

The purpose of this research is the fundamental research of hydrogen recycling and plasma detachment utilizing end loss plasma of GAMMA 10/PDX as shown below. The state of desorbed hydrogen molecules in hydrogen recycling is clarified, in order to contribute to the understanding of physical phenomena in the edge plasma and estimation of the density distribution of the future devices. The behavior of hydrogen in plasma detachment caused by MAR is clarified, in order to contribute to the unified understanding of atomic and molecular processes of MAR and its physics.

Outline of the thesis is as follows; after introducing the first chapter, Chapter 2 describes the atomic and molecular processes of hydrogen plasma associated with hydrogen recycling and plasma detachment. In the chapter 3, GAMMA 10/PDX and the divertor simulation experimental module (D-module) is described. In the chapter 4, results of experiment of hydrogen recycling in the divertor simulation plasma utilizing high-temperature tungsten target and end loss plasma. In chapter 5, experimental result of plasma detachment caused by molecular activated recombination is described. In chapter 6, experimental result of the response of plasma detachment caused by MAR to plasma density modulation is described. Finally, this thesis is concluded in the chapter 7.

Chapter 2
Atomic and molecular processes of hydrogen plasma

In this research, emission spectra from hydrogen atoms and hydrogen molecules are measured. In this section, the energy structure of hydrogen, elementary processes of hydrogen atoms and molecules, and emission from hydrogen molecules (Fulcher-α band) and hydrogen molecular ro-vibrational temperature evaluation method which used Fulcher-α band are introduced.

2.1 Characteristics of hydrogen atoms and molecules

2.1.1 Electron energy levels of atom and molecular

It is understood out that electrons around the atomic nucleus exist only in the orbit of a certain radius by solving Schrodinger's equation on the state of electrons around the nucleus. The eigenvalue of energy of the hydrogen atom is represented as follows

$$E_n = -\frac{me^4}{2(4\pi\varepsilon_0)^2\hbar^2}\frac{1}{n^2} \ , \tag{3.1}$$

where,
n : Principal quantum number
e : Elementary charge
e_0: Dielectric constant under a vacuum
$\hbar$: Reduced Planck constant.

The orbital electrons of energy with the minimum is called ground level, and the principal quantum number is n=1. The hydrogen atom with that state is called ground state. The level with an energy higher than the ground level (n>1) is called an excitation level and atoms in this state is called the excited state. Hydrogen atoms in the ground state transition to the excitation level (i.e. upper level) by receiving energy from the outside. The atoms in the excited state transit to the state of lower level (i.e. de-excitation) and photons with energy equal to the difference between the energy levels are emitted. The emission spectrums associated with the

transition from n>3 → n=2 are called Balmer series (e.g. n=3 → n=2: Balmer-α, n=4 → n=2: Balmer-β, n=5 → n=2: Balmer-γ, *etc.*).

The energy structure of hydrogen molecules has the electronic state, vibrational state and rotational state [63]. The energy eigenvalue of vibrational state and rotational state are associated with the interaction between the orbital electron and the nucleus, and its Schrödinger equation cannot be analytically solved because it is a many-body problem. Since the motion of vibration and rotation of nuclei are much slower than the movement of electrons, the Born-Oppenheimer approximation which handles each movement separately is adapted [64]. The nuclei movement of vibration and rotation are obtained by analytically solving the Schrödinger equation for each nucleus with the Born-Oppenheimer approximation. The states of electrons cannot be analytically solved because the interaction between each electron and the interaction between nuclei and electrons must be taken into consideration. The state of electrons in a molecule are understood by using the Valence Bond method and the Molecular Orbit method [65]. Fig. 3.1 shows the potential energy of the hydrogen molecule. There are vibrational levels in each electronic level and there are rotational levels in each vibrational level, respectively as shown in Fig. 3.1. The vibrational states in the electronic excitation state are referred to as the vibronic state. The inter-nuclear distance before and after the transition of the electronic state is considered to be not changed because the transition of electronic state occurs in rather short time compared with the movement of nuclei. The transition from one electronic state to another rovibronic state is expressed as a vertical movement as shown in Fig. 3.1, and which is called as Franck–Condon principle. The potential energy calculated by the Molecular Orbit method is often have been compared with the experimental result on emission spectrums associated with the transition of an electron from a higher state to a lower state [66].

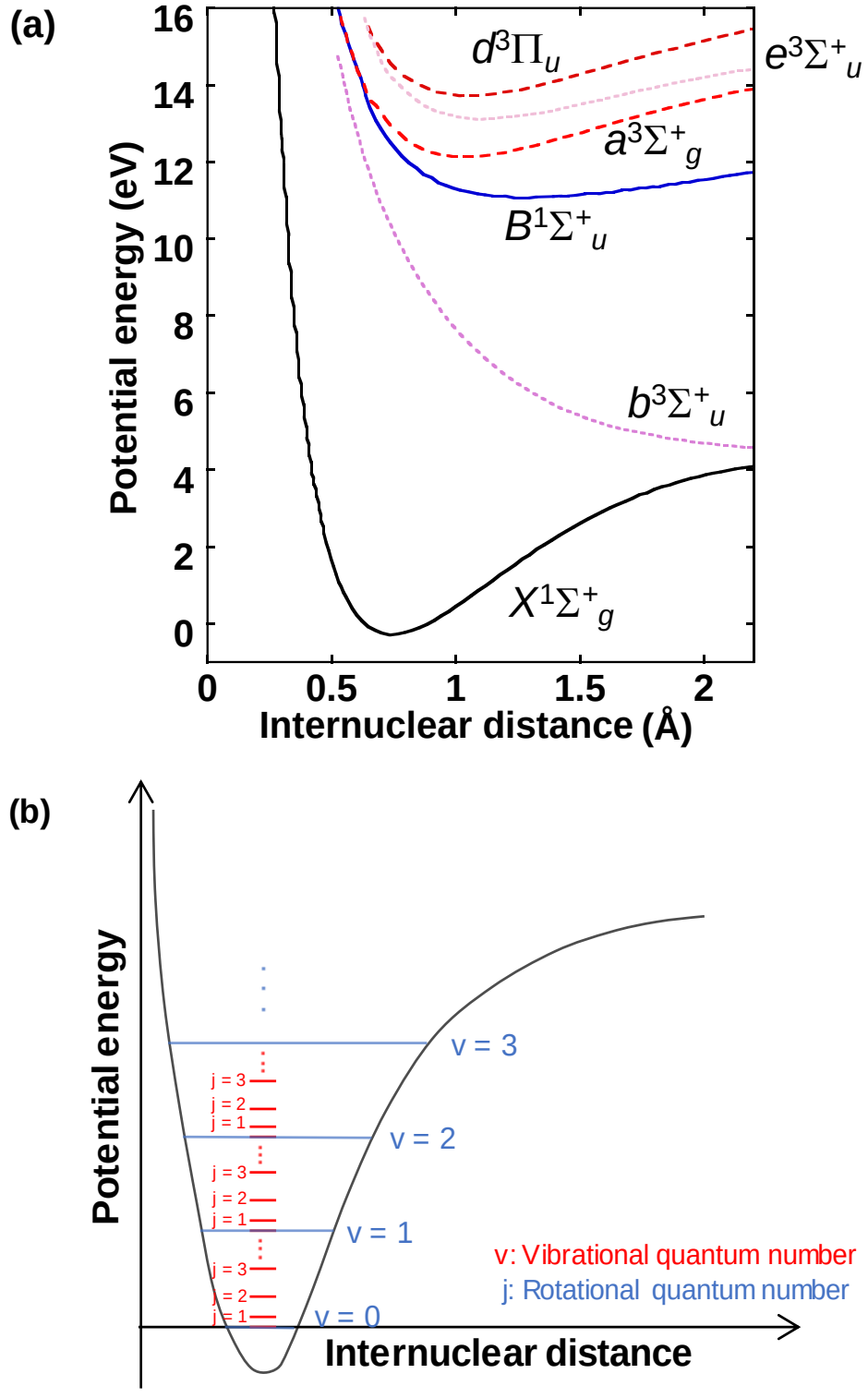

Fig.3.1 (a) Potential curves for a hydrogen molecule and (b) Schematic drawing of potential curve of H_2 in the ground electronic state.

2.1.2 Atomic and Molecular reactions

In the hydrogen plasma, hydrogen neutrals exist in the form of atoms and molecules and which are undergone elastic collision and inelastic collision with charged particles in the plasma. Regarding the inelastic collision of hydrogen atoms [67], electron impact excitation, ionization, recombination and charge exchange reaction are shown below.

Excitation :	$H + e \rightarrow H^* + e$	(3.2)
De-excitation :	$H^* + e \rightarrow H + e$	(3.3)
Ionization :	$H + e \rightarrow H^+ + e + e$	(3.4)
Radiative recombination :	$H^+ + e \rightarrow H + h\nu$	(3.5)
Three-body recombination :	$H^+ + e \rightarrow H^* + e$	(3.6)
Charge exchange :	$H + H^+ \rightarrow H^+ + H$	(3.7)

Excitation and ionization of hydrogen atoms are mainly caused by collisions with electrons which has energy higher than the excitation energy and ionization energy. The reaction of (3.3) is the transits to the lower level due to electron collision and which is called electron collision de-excitation. The recombination reaction occurs when electrons close to the hydrogen ion and captured in the electron orbit. In the radiative recombination, electrons are captured in the electron orbit and emit a photon which has the excitation energy and the kinetic energy of the electron. In the three-body recombination, excited atoms are produced due to the third electron is received kinetic energy which should be emitted by radiative recombination. Radiative recombination occurs in the plasma which is low-temperature and low-density, and the three-body recombination occurs in the plasma which is low-temperature and high-density plasma. In the charge-exchange reaction, an electron in the atom is received to the ion in the plasma, and atom had the kinetic energy of ions are produced.

In the inelastic collisions of hydrogen molecular, there are reactions with dissociation and without dissociation [67]. The transition to the upper vibronic state by electron collision and rotational excitation due to ion collision are the reactions without dissociation as shown below. The cross-section of these largely depends on the vibrational level.

Non-dissociative excitation	: $H_2(X^1\Sigma_g^+ ; v, j) + e \rightarrow H_2^*(v', j') + e$	(3.8)
Dissociative excitation	: $H_2(X^1\Sigma_g^+) + e \rightarrow H_2(\text{b-triplet}) + e \rightarrow H(1s) + H(1s)$	(3.9)
Dissociative ionization	: $H_2 + e \rightarrow e + H_2^+ \rightarrow e + H^+ + H + e$	(3.10)

The reaction with dissociation occurs due to the process which transition to the upper vibronic state by electron collision then transit to the dissociative state (e.g. b-triplet). When an electron in the hydrogen molecules obtains the potential energy larger than the dissociative level, the difference between dissociation energy and potential energy (i.e. Franck–Condon energy) is

distributed to each dissociated atom as kinetic energy. The above-mentioned process is called the Franck-Condon Process. The atom (H(1s)) dissociated from b-triplet state has a kinetic energy of around 3 eV by the Franck-Condon Process.

The process of hydrogen molecules with ionization is shown below.

Electron impact ionization : $H_2 + e \rightarrow H_2^+ + e + e$ (3.11)

The hydrogen molecules ion (H_2^+) is also produced by charge exchange reaction of hydrogen molecules with ions as shown below.

Chaege exchange : $H_2 + H^+ \rightarrow H_2^+ + H$ (3.12)

When an ion close to a molecule, the dipole moment is produced due to the molecule is polarized by the electric field of an ion. The charge exchange reaction of hydrogen molecules has the characteristic that the collision cross-section is rather large and does not depend largely on the kinetic energy of the ions, because the attractive potential acting between induced dipole and ions is proportional to the minus fourth power of the distance.

On the other hand, H3+ is produced by collision with H2+ and hydrogen molecules as shown below.

Dissociative ionization : $H_2 + H_2^+ \rightarrow H_3^+ + H_2$ (3.13)

As shown below, H2+ and H3+ recombine with electrons in the plasma (i.e. Dissociative recombination).

Dissociative recombination (DR2) : $H_2+ + e \rightarrow H(1s) + H(n\geq 2)$ (3.14)

Dissociative recombination (DR3) : $H_3+ + e \rightarrow H_2(v) + H(n\geq 1)$, (3.15a)

$H(1s) + H(1s) + H(1s)$ (3.15b)

The DR2 reaction (3.14) produces atoms with the ground state and excited state. The DR3 reaction (3.15) has two reaction branches, and that branching ratio depends on the electron energy. The branching ratio which the excited molecules and the excited atoms (3.15a) produced are larger than the branching ratio which the three atoms (3.15b) produced when the electron energy is around 1 to 7 eV. Hydrogen negative ion is produced by the electron dissociative attachment reaction as shown below. The cross-section of electron dissociative attachment reaction depends strongly on the vibrational excitation level and rotational excitation level of hydrogen molecules. It plays an important role in the molecular activated recombination as

discussed below. Also, that reaction has been utilized for the production of negative ion in the volumetric negative ion source.

In addition, recently, it is investigated that negative ions are produced by the resonant ionization process [68, 69]. Resonant ionization process is shown below.

$$H(2s) + H(2s) \rightarrow H^+ + H^-(2l2l') \quad (3.17)$$

$$H^+ + H^-(2l2l') \rightarrow H_2^{**} \quad (3.18)$$

$$H_2^{**} \rightarrow H^+ + H^-(1s^2) \quad (3.19)$$

The resonant ionization process has been recently attracted new interest for the production of negative ions in the volumetric negative ion source. The yield of negative ions increases when alkali metal (e.g. cesium) is applicated on the inner wall of the vacuum vessel of the negative ion source [70], however that cause have been not completely clarified. The promotion of negative ion yield considered to be associated with the resonant ionization process of H(2s) produced by the alkali metal [71].

The mutual neutral reaction between hydrogen negative ions and positive ions is shown below.

$$\text{Mutual neutralization (MN)} \quad : H^- + H^+ \rightarrow H(n=2, 3) + H(1s) \quad (3.20)$$

$$\text{Mutual neutralization (MN2)} \quad : H^- + H_2^+ \rightarrow H(n\geq 2) + H_2(v) \quad (3.21)$$

These reactions which is destruction of negative ions, have been investigated to make utilization of molecular activation recombination discussed below and the increase in negative ion yield in the negative ion sources [72]. The excited atom and ground state atom are produced by mutual neutralization of negative ion and positive ion and which has a large cross-section for the H(n=3) production. The excited atom and vibrationally excited molecules are produced by mutual neutralization of negative ions and molecular ions [73]. The MN2 reaction has a large cross-section for the H(n=5) production [73].

2.1.3 Fulcher-α band

Fulcher-α band is the emission spectrums associated with spontaneous emission from the state of d3πu to the state of $a^3\Sigma_u^+$ in the hydrogen molecule, which is visible light emission with wavelength of 590 to 640 nm. In the plasma, hydrogen molecules in the electronic ground state ($X^1\Sigma_g^+$) are excited to the vibronic state of $d^3\Pi_u$ by electron collisions. The vibrational excitation level and the rotational level in the $d^3\Pi_u$ state are defined as v' and j', and the vibrational level and rotational level in the $a^3\Sigma_u^+$ state are defined as v'' and j'', respectively. The transitions associated with the Fulcher-α band are v' = v'', and transitions of j'=j'', j'=j''-1 and j'=j''+1 are

called Q-branch, R-branch and P-branch, respectively (i.e. Δj=0: Q branch, Δj=-1: R-branch, Δj=+1: P-branch). The emission intensity of the Fulcher-α band associated with v'≥4 is rather low because there is the dissociation limit to H(1s) and H(2s) between v'=3 and v'=4 which leads to pre-dissociation. There are abnormalities in the emission intensity of P-branch and R-branch because $d^3\Pi_u^+$state related R-branch and P-branch transition to the state of $e^3\Sigma_u^+$ with non-radiative [74]. The population density distribution of the vibrational level and rotational level in the $d^3\Pi_u$ state can be obtained from the emission intensity of the Q-branch. In the low-density plasma, the population density distribution of the vibrational level and rotational level in the electronic ground state ($X^1\Sigma_g^+$) can be estimated from the emission intensity of Q-branch [75] as mentioned below.

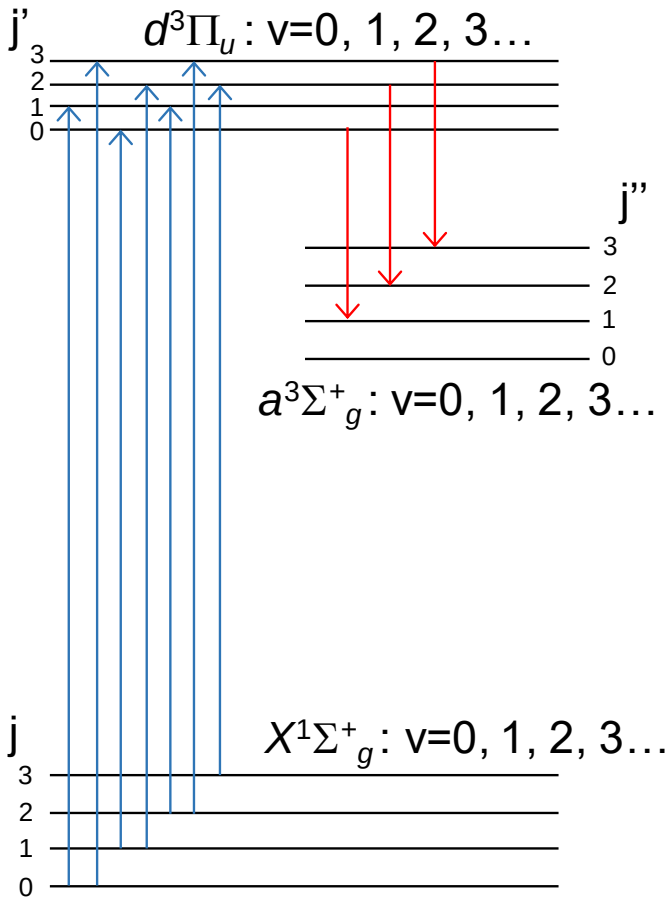

Fig.3.2 (a) Selection rule for Fulcher-α band.

2.1.4 Vibrational and rotational temperature of hydrogen

The corona model can be used to estimate the population density, and it is only taken into account the electron impact excitation from the lower level and the spontaneous emission [76]. Meanwhile, CR-model is used when there is population inflow or outflow other than electron impact excitation and spontaneous emission (e.g. ionization and recombination) [76]. Here we

will describe the estimation method of population density distribution about vibrational level and rotational level in the electronic ground state of hydrogen molecules.

In low-density plasma (e.g. $n_e \leq 10^{18}$ m^{-3}), the collision frequency of electron impact with hydrogen molecules at the state of $d^3\Pi_u$ and $a^3\Sigma_u^+$ is rather small. Hence, the emission intensity of Fulcher-α band shoud be considered only with the inflow into the $d^3\Pi_u$ state due to electron impact such as $X^1\Sigma_g^+ \rightarrow d^3\Pi_u$ and the outflow from $d^3\Pi_u$ state such as $d^3\Pi_u \rightarrow a^3\Sigma_u^+$. The population density of the vibrational level and rotational level of $X^1\Sigma_g^+$ state (N_{Xvj}) is shown in below.

$$\frac{\partial N_{dv'j'}}{\partial t} = n_e \sum_{v,j} \left[N_{Xvj}^{dv'j'} R_{Xvj}^{dv'j'} \right] - N_{dv'j'} \sum_{v",j"} A_{av"j"}^{dv'j'} \quad , \tag{3.22}$$

where,

$N_{dvj'}$: Ro-vibrational population density of $H_2(d^3\Pi_u)$

$N_{Xvj}^{dvj'}$: Ro-vibrational population density of $H_2(X^1\Sigma_g^+)$

$R_{Xvj}^{dvj'}$: Rate coefficient of electron impact ionization such as $X^1\Sigma_g^+ \rightarrow d^3\Pi_u$

$A_{av"j"}^{dvj'}$: Spontaneous coefficient of $d^3\Pi_u \rightarrow a^3\Sigma_u^+$.

The equation (3.22) can be deformed as shown in below with applying the quasi-steady-state (QSS) approximation.

$$n_e \sum_{v,j} \left[N_{Xvj}^{dv'j'} R_{Xvj}^{dv'j'} \right] = N_{dv'j'} \sum_{v",j"} A_{av"j"}^{dv'j'} \tag{3.23}$$

Besides, the emission intensity of Fulcher-α band ($I_{av"j"}^{dv'j'}$) shown below.

$$I_{av"j"}^{dv'j'} = \frac{hc}{\lambda_{av"j"}^{dv'j'}} N_{dv'j'} A_{av"j"}^{dv'j'} \tag{3.24}$$

Where,

h: Planck constant

c: Light velocity

$\lambda_{av"j"}^{dv'j'}$: Wavelengths of Fulcher-a band.

From equations (3.23) and (3.24), $I_{av"j"}^{dv'j'}$ can be convert as shown below.

$$I_{av''j''}^{dv'j'} = \frac{hc}{\lambda_{av''j''}^{dv'j'}} \frac{A_{av''j''}^{dv'j'}}{\sum_{v'',j''} A_{av''j''}^{dv'j'}} n_e \sum_{v,j} \left[N_{Xvj}^{dv'j'} R_{Xvj}^{dv'j'} \right] \quad (3.25)$$

The population distribution of vibrational and rotational level in the electronic ground state can be associated with the emission intensity of the Fulcher-α band. Equation (3.25) can be described as (3.26) by assuming that the density distribution of vibrational and rotational level in $X^1\Sigma_g^+$ follows the Boltzmann distribution of T_{biv} and T_{rot}.

$$I_{av''j''}^{dv'j'} = \frac{hc}{\lambda_{av''j''}^{dv'j'}} \frac{A_{av''j''}^{dv'j'}}{\sum_{v'',j''} A_{av''j''}^{dv'j'}} n_e \sum_{v,j} R_{Xvj}^{dv'j'} C_{Xv}(2j+1) g_{as}^{j} exp\left[-\frac{F_X(v,j)}{kT_{rot}^X} - \frac{\Delta G_X(v)}{kT_{vib}^X} \right] \quad (3.26)$$

Where,

g_{as}^{j}: The spin multiplicity of molecule

$F_x(v, j)$: Rotational energy

$\Delta G_x(v)$: Vibrational energy subtracted by zero-point energy

T_{rot}: Rotational temperature

T_{vib}: Vibrational temperature

C_{xv}: The constant set so that the summation of j becomes population density of v, as shown below,

$$C_{Xv} = \frac{1}{\sum_j (2j+1) g_{as}^{j} exp\left[-\frac{F_X(v,j)}{kT_{rot}^X} \right]} . \quad (3.27)$$

In this study, T_{vib} and T_{rot} were obtained by applying the emission intensities of Fulcher-α to the equation of (3.26) [75].

2.2 Hydrogen recycling

Ions and neutral particles incident on the plasma facing material are almost reflected and others are diffused in the bulk. The hydrogen diffused in the material is captured inside the material, and others reach the material surface via the diffusion. Hydrogen reached the surface of bulk recombine with another hydrogen and it becomes a molecule, which is released to the plasma (i.e. surface recombination). The circulation of hydrogen between the plasma and the plasma-facing wall mentioned above is called hydrogen recycling.

In the long plasma discharge in the torus devices, the inner vessel wall continues to retain hydrogen. As a result, the rate of exhausted hydrogen from the vacuum vessel becomes smaller than the rate of supplied hydrogen to the vacuum vessel. The particle balance in the vacuum vessel is described as shown below.

$$\frac{\partial N_H^0}{\partial t} + \frac{\partial N_H^p}{\partial t} = \Gamma_{fuel} - \Gamma_{pump} - \Gamma_{wall} \tag{3.27}$$

where,

N_{H^0}: Neutral atoms in the vacuum vessel

N_{H^p}: Ions in the vacuum vessel

Γ_{fuel}: The number of hydrogen atoms supplied the vacuum vessel per unit time

Γ_{pump}: The number of hydrogen atoms exhausted from the vacuum vessel per unit time

Γ_{wall}: The number of hydrogen atoms adsorbed into the wall per unit time.

In several tokamak experiments, an overall increase in the amount of hydrogen released from facing-wall associated with the increase in the temperature of facing-wall has been observed (i.e. global-wall saturation) [55-60]. In the case of wall saturation, Γ_{wall} in the equation (3.27) has a positive value, and density control becomes difficult due to the number of hydrogen particles in the vacuum chamber continues to increase without hydrogen supply. Hydrogen released from plasma-facing wall is considered to be mainly molecular state because of the reflection coefficient of hydrogen on the plasma-facing wall nearly independent of the wall temperature. Hence, it is important to know the amount and state of desorption molecules for stable plasma operation.

The Eley-Rideal (ER) mechanism and the Langmuir-Hinshelwood (LH) mechanism [77], which are the process of surface recombination, are shown below.

ER : $H_{gas} + surface \rightarrow H_{ad}$ (3.28a)

$H_{ad} + H_{gas} \rightarrow H_2(v,j)_{gas}$ (3.28b)

LH : $H_{ad} + H_{ad} \rightarrow H_2(v,j)_{gas}$ (3.29)

where,

H_{gas}: Hydrogen atoms in the plasma

H_{ad}: Hydrogen atoms adsorbed on the bulk of surface

$H_2(v,j)_{gas}$: Desorbed hydrogen molecular from bulk of surface.

In both mechanisms, the desorbed molecules are in the vibrationally and rotationally excited states. In the ER mechanism, ions and atoms in the plasma are adsorbed on the bulk surface, then it recombines with other hydrogen atoms on the bulk surface and desorbs from the bulk surface as molecules. In the LH mechanism, atoms adsorbed on the bulk surface are recombined with each other into molecules and which desorbs from the bulk surface. Actually, the molecule desorbs by the mechanism which is a combination of two schemes mentioned above, which is the so-called hot-atom recombination mechanism [61] as shown below, because these two mechanisms are considered to be as two ideal limits.

Hot-Atom recombination : $H_{gas} + surface \rightarrow H_{hot}$ (3.30a)

$H_{hot} + H_{ad} \rightarrow H_2(v,j)_{gas}$ (3.30b)

where,
H_{hot}: Hot hydrogen atoms on the bulk of surface.

The hot atoms (H_{hot}), which can easily move on the surface react with each other before full thermalization. Consequently, the vibrational level and rotational level of the desorption molecule have a distribution (i.e. T_{vib} and T_{rot}). It has been reported that the vibrational temperature of molecules which desorbed from the surface is determined by the material and its surface condition [78].

2.3 Molecular activated recombination (MAR)

In the production of detached plasma, it is important to cause the recombination reaction much more than ionization. In the plasma recombination process, there are electron-ion recombination (EIR) and molecular activation recombination (MAR) which is involved with various reaction associated with molecules. In the case that the electron temperature has less than around 1 eV, the reaction rate coefficient of EIR has larger than ionization. Whereas the reaction rate coefficient of MAR has much larger than ionization for the of $T_e \leq 3$ eV [43]. Accordingly, MAR has been investigated experimentally and theoretically for the achievement of more effective plasma detachment [35, 43, 44].

The reaction processes of MAR in the hydrogen plasma are shown below.

IC-MAR:

CNV/CX : $H_2(v) + H^+ \rightarrow H_2^+ + H$ (3.31a)

DR2 : $H_2^+ + e \rightarrow H + H(n \geq 2)$ (3.31b)

MIC-MAR:

CNV/CX : $H_2(v) + H^+ \rightarrow H_2^+ + H$ (3.32a)

CNV2 : $H_2(v) + H_2^+ \rightarrow H_3^+ + H$ (3.32b)

DR3 : $H_3^+ + e \rightarrow H_2(v) + H,$
$H_2^*(v) + H,$
$3H$ (3.32c)

DA-MAR:

DA : $H_2(v) + e \rightarrow H^- + H$ (3.33a)

NM : $H^- + H^+ \rightarrow H + H(n=2,3).$ (3.33b)

In the IC-MAR process, hydrogen molecular ion (H_2^+) is produced by the reaction of CNV and CX, and it recombines into excited atom and ground state atom in the DR2 reaction. Similarly, in the MIC-MAR, hydrogen tri-atomic molecular ion is produced by the reaction of CNV2, and it recombines with in the DR3 reaction. In the DA-MAR process, negative ion (H^-) is produced by dissociative attachment with an electron, and it mutual neutralize with ion into excited atom and ground state atom.

The volume recombination associated with EIR and MAR had been observed in the NAGDIS-II divertor simulator at Nagoya University [30]. In the experiment mentioned above, it has been observed that continuous spectrum associated with three-body recombination and emission from highly excited atoms during helium detachment plasma [30]. On the other hand, these emission spectrums have not been observed during hydrogen detachment plasma associated with MAR [79]. The negative hydrogen ions have been observed during detached plasma by MAR in divertor simulator MAP-II [80, 81]. In the experiments of MAP-II, it was revealed that the contribution of mutual neutralization between hydrogen negative ion and the positive ion is rathar large from results of spectroscopic measurement [34]. Hydrogen ions (e.g. H_2^+, H_3^+) has been observed in the low-density hydrogen plasma by the omegstron-type mass spectrometer in PISCES-A at UCSD [47]. In addition, hydrogen negative ion and hydrogen molecular ions have been measured and their contribution to MAR have been investigated in a linear divertor simulator TPD-Sheet IV at Tokai University [46].

Although plasma detachment associated with MAR had been observed utilizing with several divertor simulators as above, the detached plasma due to MAR have been few observed except Alcator C-Mod [48]. The reason for MAR has not been observed in tokamaks is considered to be that the reaction of molecular activated ionization (MAI) and molecular activated dissociation (MAD) becomes dominant [49]. The reactions of MAI and MAD is shown below, and these reactions compete with the reactions of MAR.

MAI : $H_2(v) + e \rightarrow H^+ + H^+ + 2e$ (3.33)

MAD : $H_2(v) + e \rightarrow H + H^+ + e$ (3.34)

Chapter 3

Experimental setup

3.1 GAMMA 10/PDX

GAMMA 10/PDX (GAMMA 10 and GAMMA Potential-control and Divertor -simulation eXperiment) is a tandem mirror device with 27 m in total length, which is the world's largest linear device. Figure 4.1 shows the schematic view of the GAMMA 10/PDX. GAMMA 10/PDX consists of the central cell, anchor cells, plug/barrier cells and end regions [82]. In the central-cell, the main plasma is mainly produced and maintained by using ion cyclotron range of frequency (ICRF) heating and hydrogen gas puffing. The plasma discharge duration is 200 ~ 400 ms. The electron cyclotron heating (ECH) system is installed at the central-cell. It consists of a high power gyrotron which has an oscillator at 28 GHz and the antenna system with a single mirror. In this study, this system has been used to heat directly the bulk electrons in the central cell. The hydrogen plasma produced at the central-cell flows to the end region as end-loss plasma. The divertor simulation experiments have been conducted utilizing end-loss plasma as divertor simulation plasma, which is discussed in the next section.

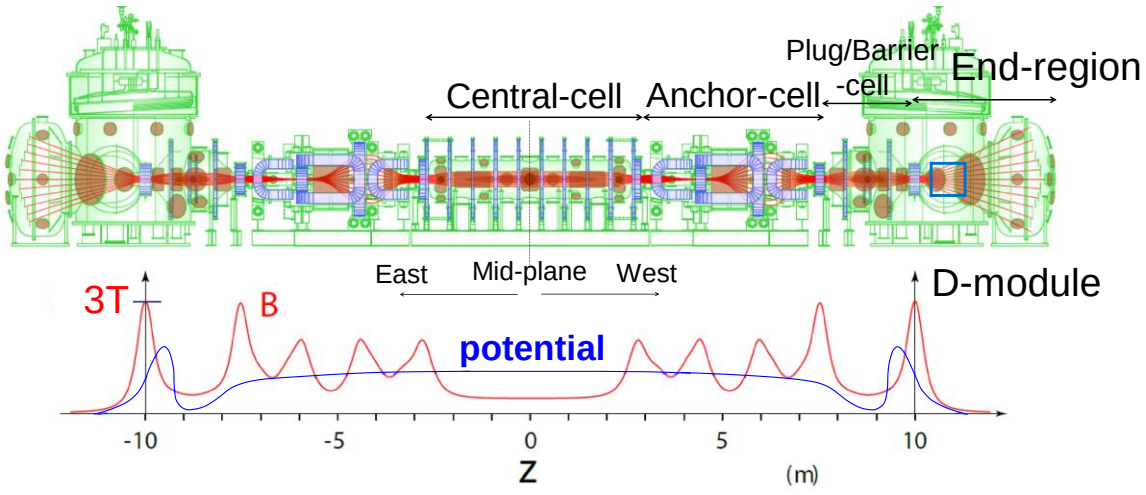

Fig.4.1 The Schematic view of GAMMA 10/PDX which viewed from the side. It shows the vacuum vessel consisted of each cell and the configuration of the magnetic field and electronic potential.

3.2 Divertor simulation experimental module (D-module)

3.2.1 Specifications of D-module

The divertor plasma phenomena and hydrogen recycling have been studied utilizing end-loss plasma as divertor simulation plasma. The Divertor simulation experimental module (D-module) is installed in the west end region as shown in Fig. 4.2. The inlet aperture of the D-module located at 0.3 m away from the end-mirror coil. The diameter of plasma is about 10 cm at the inlet aperture and 30 cm at V-shaped target plate. A quartz window is attached on a side of D-module for measuring the emission of divertor simulation plasma. Figure 4.3 shows the schematic views of the D-module and Fig. 4.4 shows a photograph of the inside of the D-module. A V-shaped target is installed inside the D-module. Sheath electric heaters and thermocouples are attached to the backside of the V-shaped target to control the temperature of the V-shaped target as shown in Fig. 4.5. A V-shaped target is covered with tungsten with the thickness of 0.2mm as the plasma-facing material. The end-loss plasma of GAMMA 10/PDX flows from the plasma inlet at the in the front panel of the D-module and the V-shaped target is exposed to the end-loss plasma. The additional gas supply port is installed near the plasma inlet to supply hydrogen gas towards the V-shaped target. The D-module can be moved up and down in the west-end mirror tank. It is set on the axis of GAMMA 10/PDX in the divertor simulation experiment.

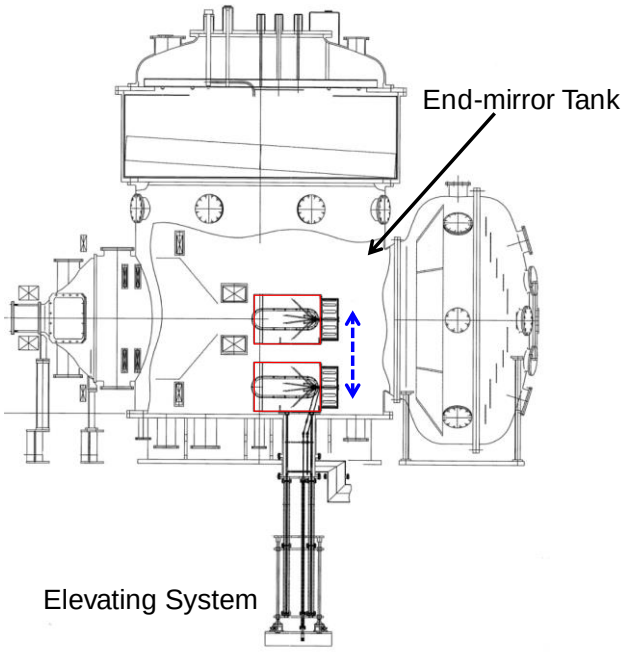

Fig.4.2 The Schematic view of the west end region of GAMMA 10/PDX which viewed from the side. The D-module is installed in the west-end region.

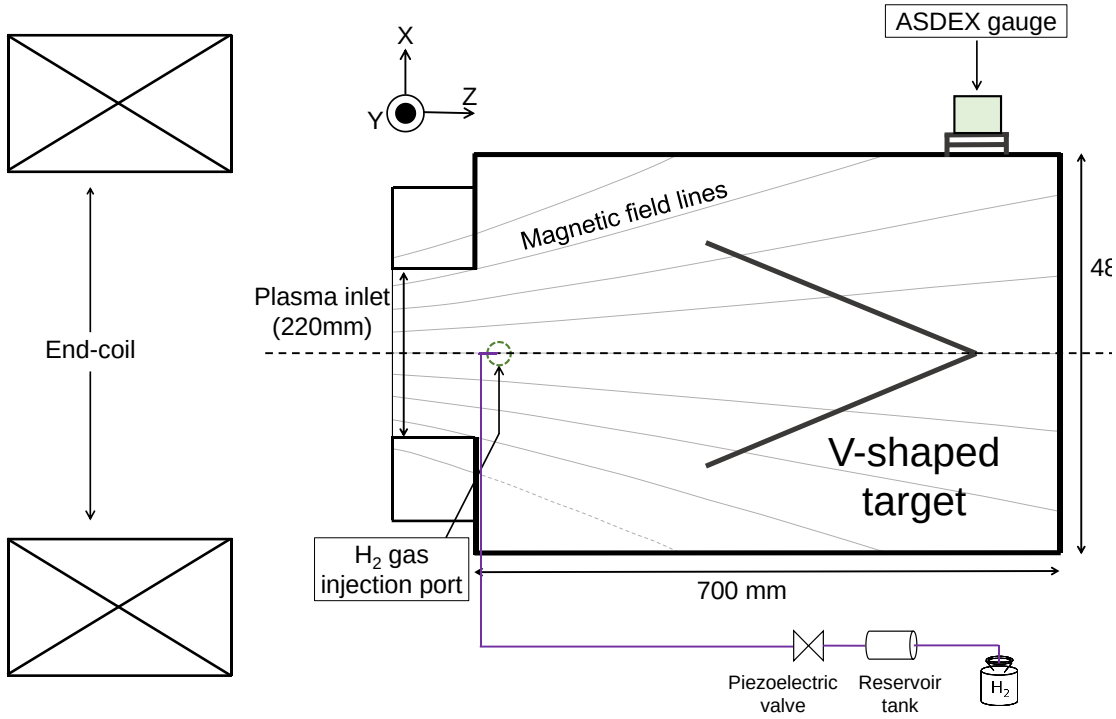

Fig.4.3 Schematic views of the D-module.

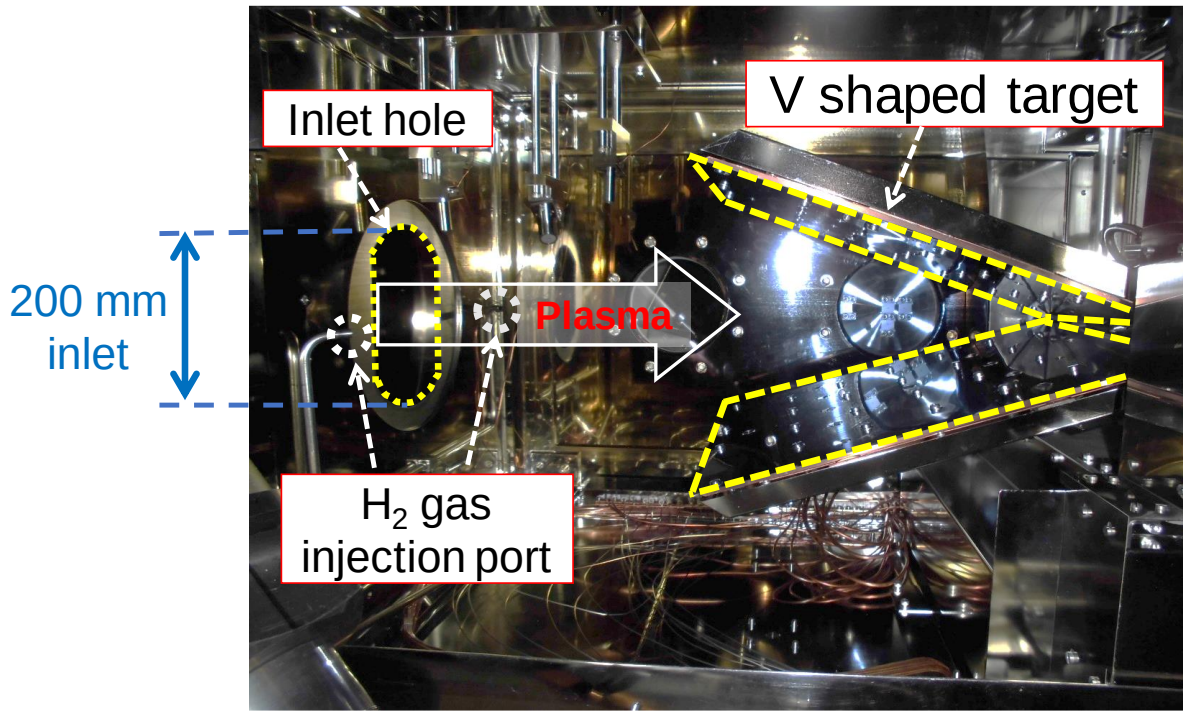

Fig.4.4 The photograph of the inside of the D-module.

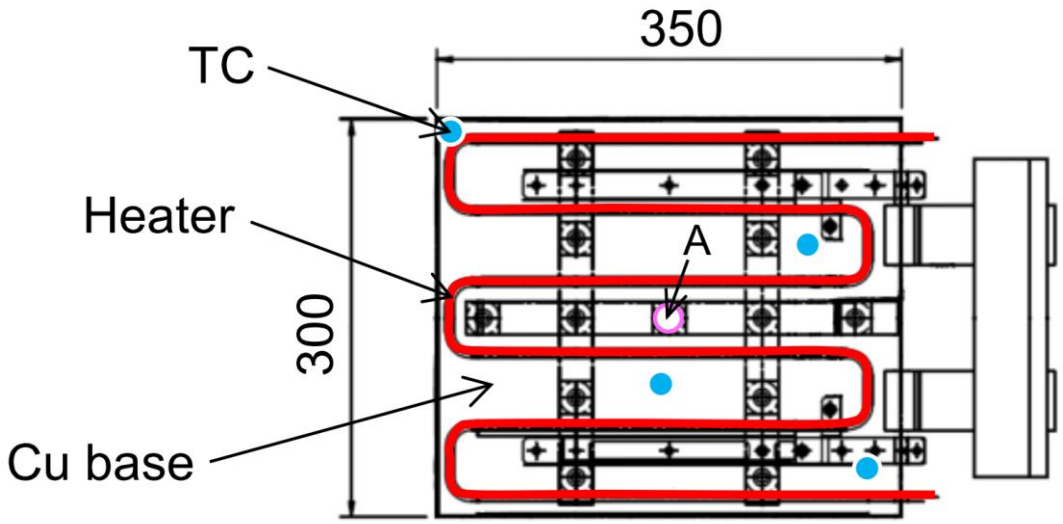

Fig.4.5 Schematic views of backside of the V-shaped target base

3.2.2 Plasma diagnostics

Spectrometers are installed in the D-module and west-end region. The line of sight and view spots of spectrometers are shown in Fig. 4.6. Hydrogen Balmer line intensities are measured with low-dispersion spectrometer (USB2000+, Ocean optics). A collimator lens is installed in the aperture of the fiber of USB2000+ which directed to the inside of the D-module. The view spot of USB2000+ is collimated in parallel which has a diameter of 480mm×500mm×700mm. Fulcher-alpha band spectrums and Balmer emissions from highly excited hydrogen atom are measured with high-dispersion spectrometer (SR500i, ANDOR) The view spots of SR500i are defined as No. 1 to No. 5 from the corner of the V-shaped target toward the upstream as shown in Fig. 4.7. The relative sensitivities of the spectrometers were calibrated with a standard lump. Thirteen Langmuir probes are installed on the surface of the upper target plate [83] as shown in Fig. 4.7. The electrode of the probe is made of tungsten and its length and diameter are 1.1 mm and 1.5 mm respectively. In this study, electron temperature (T_e) and electron density (n_e) are measured using Langmuir probes.

The high-speed camera (MEMRECAM GX-1, NAC Inc.) is installed in the west-end region as shown in Fig. 4.6. The data obtained with GX-1 is the monochrome scale with 8 bits depth. GX-1 with a frame rate of 1000~20000 fps is used to measure the spatial distribution and time evolution of the emission from diverter simulation plasma. Two-dimensional images of the hydrogen Balmer-alpha intensity ($I_{H\alpha}$) and Balmer-beta intensity ($I_{H\beta}$) in front of the V-shaped target are measured with a high-speed camera with an interference filter in front of the lens. The center wavelengths of the transmittance profile of the interference filter for $I_{H\alpha}$ and $I_{H\beta}$ are 656 nm and 486 nm, respectively, and the full width at half maximum of both filters are around 10 nm.

The ASDEX type fast ionization gauge (ASDEX gauge) is installed on the top of the D-module [84] as shown in Fig. 4.3. The ASDEX gauge can measure the neutral pressure in a magnetic field and is used for measuring the neutral gas pressure in the divertor simulation plasma.

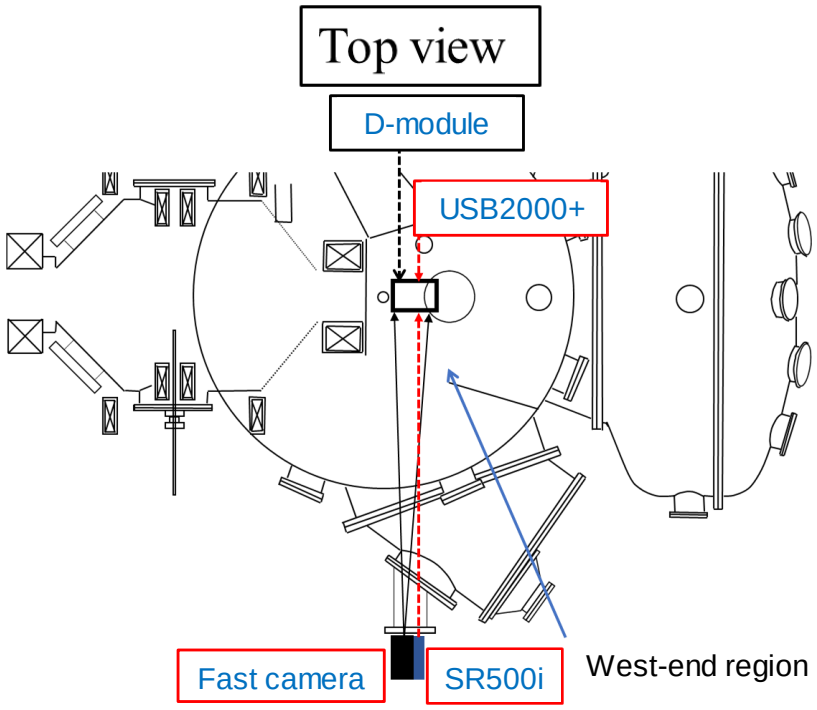

Fig.4.6 Top view of the west end region and line of sight of the spectrometers (USB2000+ and SR500i) and the high-speed camera.

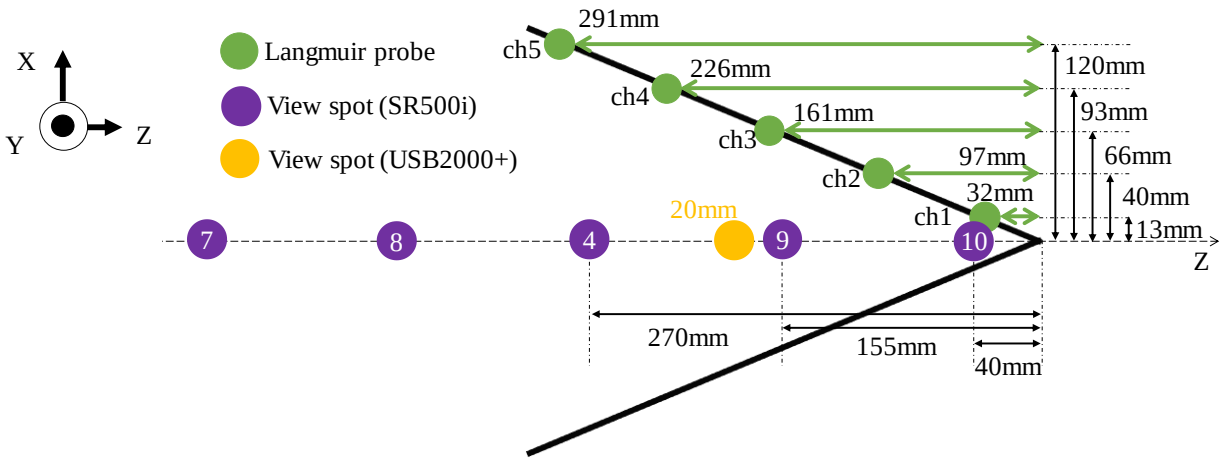

Fig.4.7 Measurement positions of Langmuir probe, USB2000+ and SR500i.

Chapter 4
Hydrogen recycling with high temperature tungsten target

In this section, the hydrogen recycling with a high-temperature target will be discussed. The enhancement of hydrogen recycling has revealed by investigating the behavior of hydrogen molecules.

4.1 Experimental method

The main plasma was produced and maintained by ICRF heating and hydrogen gas puffing at the central cell and the plasma discharge duration was 400 ms. The D-module was arranged on the z-axis, and the V-shaped target was exposed to the end loss plasma. The temperature of the V-shaped target was changed from room temperature (~300 K) to ~ 570 K by shot-by-shot, by a sheath heater attached back side of it as shown in Fig. 6.8. In this experiment, the relationship between the target temperature and plasma parameters in the D-module was obtained. The neutral gas pressure in the D-module was measured by an ion gauge installed at the top. The neutral pressure in the D-module was 5.8×10^{-7} Torr when the T_{target} was 330 K and 6.2×10^{-7} Torr when at 573 K without plasma. The increase in the neutral pressure in the D-module was 6.7%, which is low enough that outgassing can be ignored.

Figure 6.9 shows the time evolution of a typical behavior of GAMMA 10/PDX main plasma in this experiment. Plasma was discharged stably during t = 150 ~ 400 ms. After 400 ms, adjustment of additional heating was carried out to prepare for another experiment. The discharge after 400 ms, additional heating was applied in order to adjust for another experiment. In this experiment, we used data in t = 150 to 400 ms at which the plasma was stable.

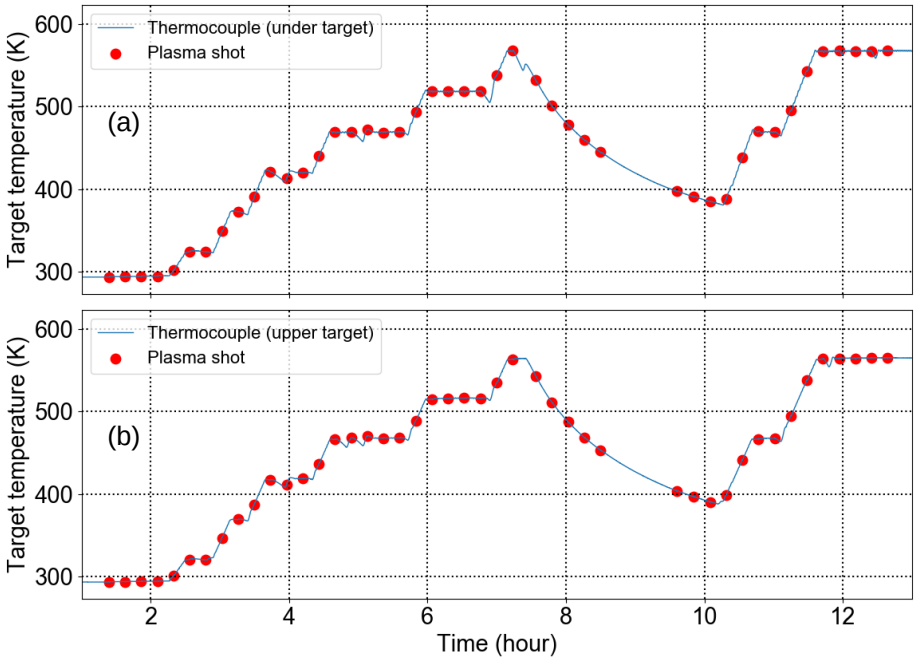

Fig.6.8 Time evolution of target temperature. (a) Upper target plate, (b) under target plate.

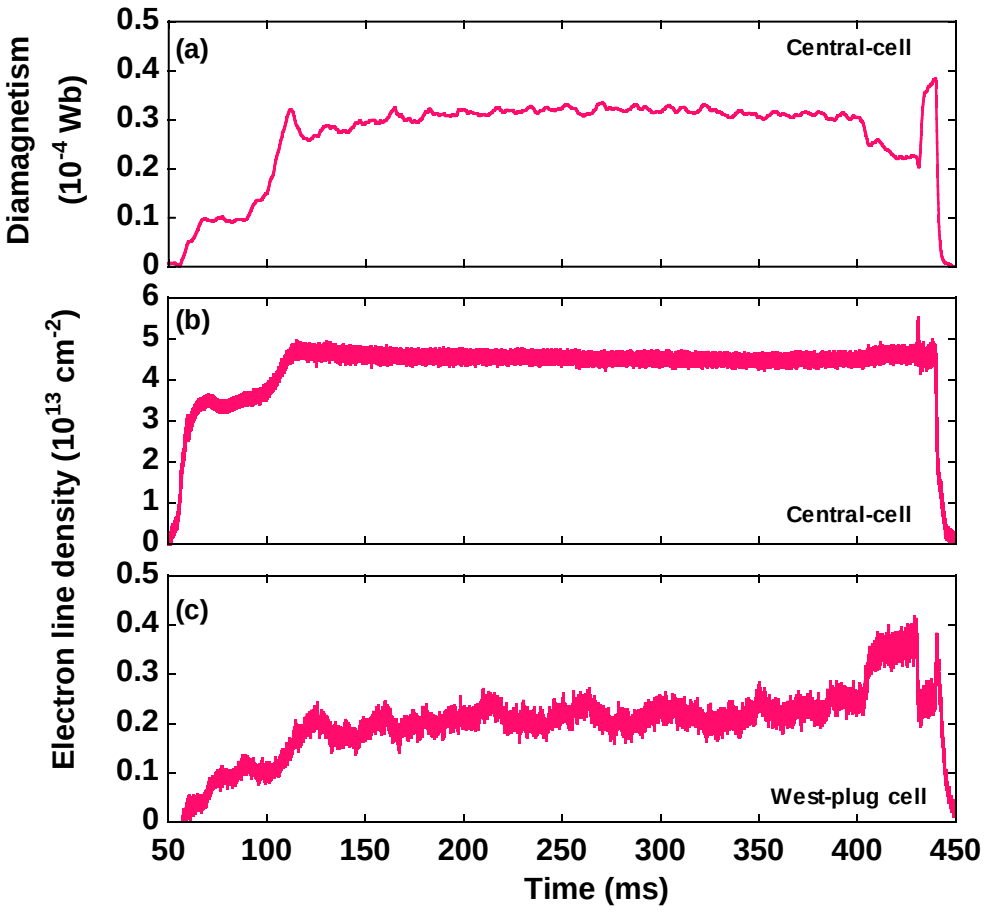

Fig.6.9 (a) Diamagnetism in the central-cell, (b) electron line density in the central-cell and (c) west-plug cell.

4.2 Experimental result and Discussion

Figure 6.10 shows the electron temperature (T_e), electron density, the intensity of Balmer series emissions ($I_{H\alpha}$ and $I_{H\beta}$) in front of the V-shaped target as a function of the T_{target}. The values of $I_{H\alpha}$ and $I_{H\beta}$ almost increased twice, though the electron density increased from ~2.3 × 10^{16} m^{-3} to ~2.6 × 10^{16} m^{-3} when the T_{target} increased from room temperature to 573 K. In other words, the increase in the Balmer-line intensities was larger than that of n_e. On the other hand, T_e was nearly constant (~30 eV), thus meaning that the rate coefficients of electron-impact excitation and ionization were not affected by the increase in T_{target}. In this plasma parameters, the mean free path for the electron-impact excitation such as H(n=1) → H(n=3) is ~100 m, which

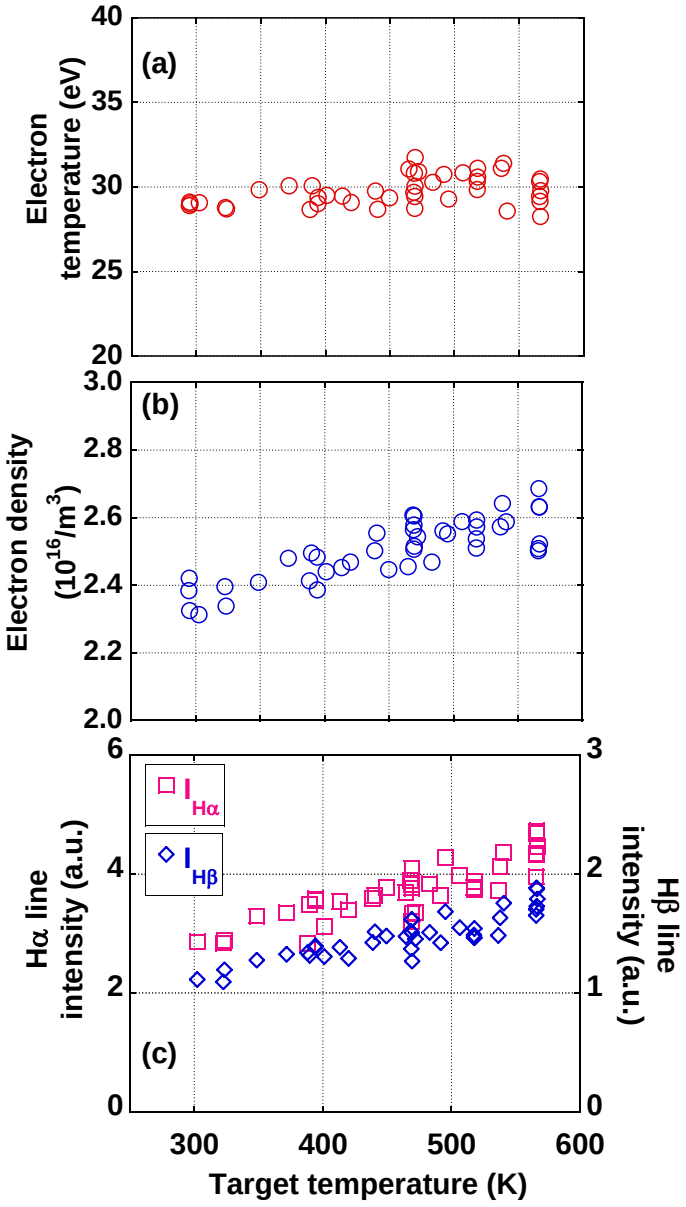

Fig.6.10 (a) Electron temperature, (b) electron density, and (c) H_α and H_β intensities measured by spectroscopy (USB2000+) as a function of the target temperature.

is longer than the dimensions of the plasma. Therefore, electron-impact excitation is not brought about the increase in $I_{H\alpha}$ and $I_{H\beta}$. The significant increase in the Balmer intensity suggests that the dissociative excitation causes the production of excitation atoms. As a mentioned in section 3.1.2, excited hydrogen atoms are produced by the electron impact dissociation of vibrationally excited hydrogen molecules, and the dissociation rate increases with the vibrational level and density of it.

Figure 6.11(a) shows a Fulcher-α band spectrum with a T_{target} of 573 K, which exposure time in this measurement was ~250 ms to increase the S/N ratio. Figure 6.11(b) shows the relative population densities of $d_3\Pi_u^-$ at 12 rovibrational states in the data of Fig. 6.11(a). The data of relative population densities are well fitted by a Boltzmann–Maxwellian distribution, and a corona model is adopted such that T_{vib} and T_{rot} are ~3400 and ~460 K, respectively. The assumption of the coronal equilibrium should be valid in low-density plasma, such as that in the present experiments (i.e. ~10^{16} m^{-3}). It means that the vibrationally excited level of the molecules is significantly higher than that expected at the thermal equilibrium between the

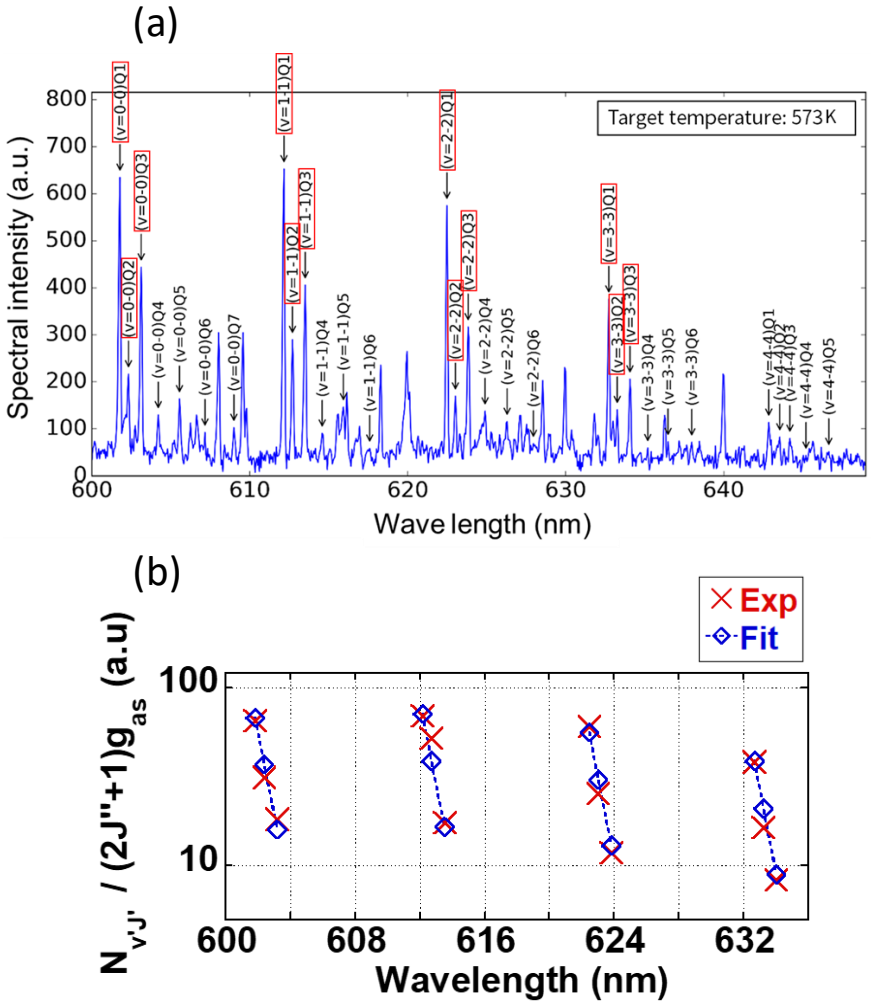

Fig.6.11 (a) Fulcher-α band spectrum and (b) relative population densities of $d^3\Pi_u^-$ for various rovibrational states at the target temperature of 573.

molecules and the target. But then these mean-free path mentioned above would be rather long due to the plasma density is rather low, thus suggesting that the desorbed molecules from the target are in the vibration excited state. Excited hydrogen molecules have been observed to be produced by atom recombination on the Cu and W materials [93], and that mechanism been proposed as Hot-Atom recombination [61, 77]. The mean free path mentioned above is estimated to be ~5 m, which is approximately one order of magnitude longer than the D-module under the present experimental conditions (i.e. $n_e = 2.5 \times 10^{16}$ m^{-3}, $T_e = 30$ eV). Hot-atom recombination on the W-target would be the dominant source of vibrationally excited molecules, although electron-impact excitation is also involved in the production of vibrationally excited hydrogen molecules.

Figure 6.12 plots T_{vib} and T_{rot} as a function of T_{target}. The rotational temperature is not equal to T_{target} moreover the rotational temperature increased with the increase in T_{target}. The difference between T_{rot} and T_{target} may be attributed to the collisions of molecules desorbed from the target with the room temperature and with high-temperature ions (~400 eV). In other words, the rotational temperature was transferred from the translational temperature equal to T_{target}. On the contrary, T_{vib} was not affected by the increase of T_{target}, thus indicating that the

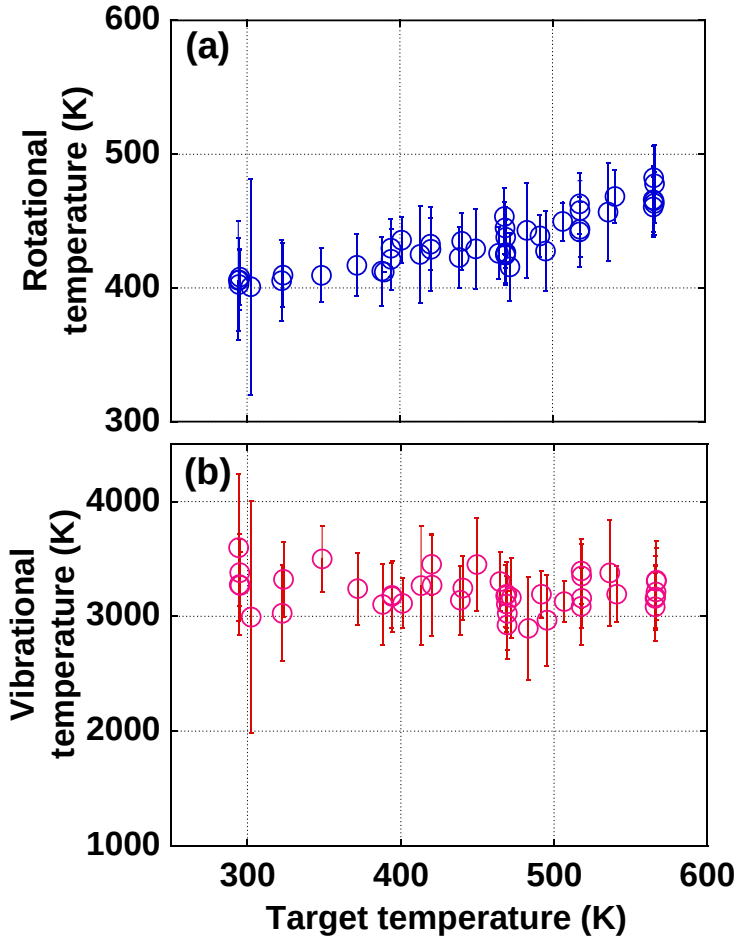

Fig.6.12 (a) Vibrational temperature (T_{vib}) and (b) Rotational temperature (T_{rot}) as a function of T_{target}.

vibrationally excited level of the hydrogen molecule was not changed by the change of T_{target}. The observation of constant T_{vib} seems to be reasonable because electron-impact excitation and hot-atom recombination do not depend on the T_{target}.

As shown in Fig. 6.13, Q1-branch intensity of the Fulcher-α band (I_{Q1}) almost increased twice when the T_{target} increased from room temperature (~300 K) to ~570 K. Figure 6,10(a) and Fig 6.12(a) shows that the density of hydrogen molecules increased with T_{target} because the intensities of the Q1-branch are proportional to the molecule density when T_e and T_{vib} are constant. The increase in the molecule density is considered to be attributed to the enhancement of surface recombination due to the increase in T_{target}. The increase in Balmer-line intensities with increasing T_{target} must be caused by the increase in the number of excited hydrogen atoms produced by the dissociation of vibrationally excited molecules desorbed from the target. The electron density may be increased caused by the ionization of these excited hydrogen atoms. The ratios of $I_{Hβ}$ to I_{Q1} are constant with increasing T_{target} as shown in Figure 6.14. When T_e and T_{vib} are constant, the ratio of $I_{Hβ}/I_{Q1}$ is a good indicator of the density ratio of hydrogen atoms to molecules [86]. The dissociation of molecules desorbed from the target was not enhanced in the case of T_{target} < 573 K, given that the ratio of densities of hydrogen atoms and molecules did not change with the T_{targe}. This finding is consistent with the result that T_{vib} remained constant with increasing T_{targe} in Fig. 6.12(b).

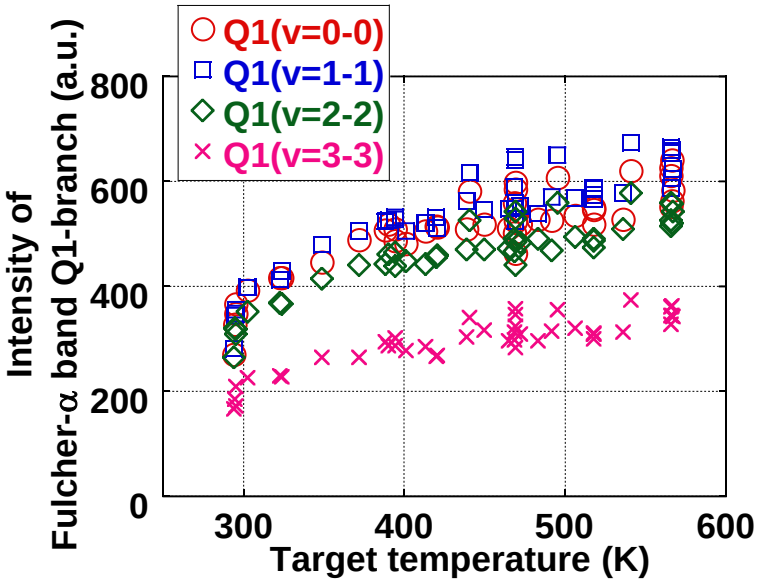

Fig.6.13 Intensity of Fulcher-α band Q1-branch as a function of T_{target}.

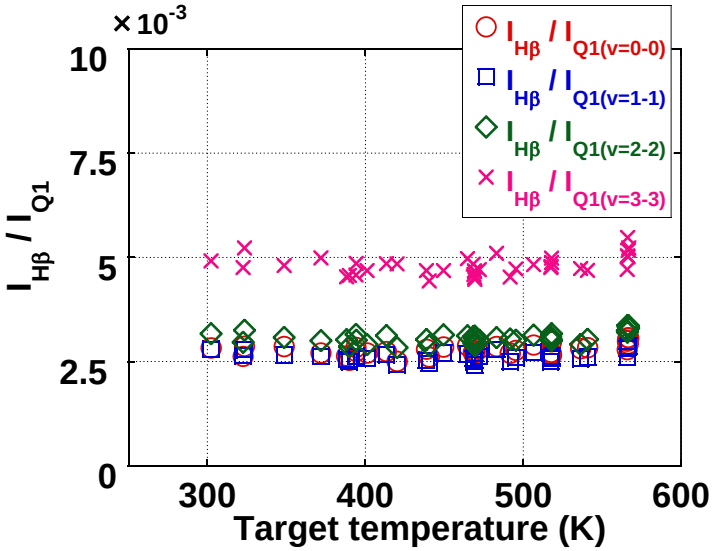

Fig.6.14 The ratio of $I_{H\beta}$ to I_{Q1} as a function of the T_{target}.

4.3 Summary

In this chapter, the behavior of hydrogen recycling in the divertor simulation plasma was discussed by the investigations of the effect of the high-temperature target on hydrogen recycling. The effect of the target temperature on hydrogen recycling was studied using a D-module with a V-shaped W target exposed to the end-loss plasma. When T_{target} was increased from room temperature to 573 K, the intensities of the H_α line, H_β line, and Fulcher-α band Q1-branch doubled even though ne increased only by ~12%, and T_e was constant. The vibrational temperature (T_{vib} = 3400 K) was significantly higher than T_{target} and remained constant, thus suggesting that the hydrogen molecules were highly vibrationally excited, and the vibrational level remained constant. The twofold increase in I_{Q1} indicates that the molecule density doubled owing to the increase in T_{target} because T_e and T_{vib} were both constant. The ratio between the densities of hydrogen atoms and molecules was also unaffected by T_{target}, thus indicating that the rate of dissociation was constant. The significant increase in Balmer-line intensities with T_{target} must be caused by an increase in the number of excited hydrogen atoms produced by the dissociation of vibrationally excited molecules, which leads to an increase in n_e, because the excited hydrogen atoms can be easily ionized by low-energy electrons. This study suggests that vibrationally excited molecules are produced by hot-atom recombination on the target. Therefore, hydrogen recycling is enhanced by the increase in the number of vibrationally excited molecules desorbed from the high-temperature wall.

Chapter 5
Plasma detachment caused by molecular activated recombination

5.1 Experimental method

In the present experiments, the main plasma is produced and maintained from t = 50 ms to t = 250 ms by ICRF in the central cell of GAMMA 10/PDX. Hydrogen gas was additionally supplied from gas supply port installed near the plasma inlet to the inside of the D-module. The gas supply duration was 500 ms such as from 300 ms before the plasma production to the end of plasma discharge. The amount of the additional hydrogen gas supply was changed shot by shot by changing the pressure in the reservoir tank (i.e. Plenum pressure) installed at the upstream of a piezoelectric valve. At each plenum pressure, the condition of the main plasma discharge was set to be the same. A plasma discharge with a relatively small diamagnetism at the central cell was performed by adjusting ICRF power and amount of gas puffing in the case of without gas supplied to the D-module, in order to minimize the influence of the gas additionally supplied into the D-module on the main plasma.

5.2 Experimental result

5.2.1 Typical behavior of the main plasma

Figure 5.1 shows the time evolution of the main plasma in the case of each plenum pressure. The main plasma was the steady state from t~100ms to t~240ms. When hydrogen gas was additionally supplied into the D-module, the diamagnetism in the central cell decreased to about 2/3 as compared with the plasma shot without additional supply. The electron line density in the central-cell was not affected by the additional gas supplying to the D-module. The electron line density in the west plug cell increased about 5 times at the maximum by the additional supply of hydrogen gas to the D-module. In this experiment, we used data of t = 100 to 200 ms at which the plasma was stable.

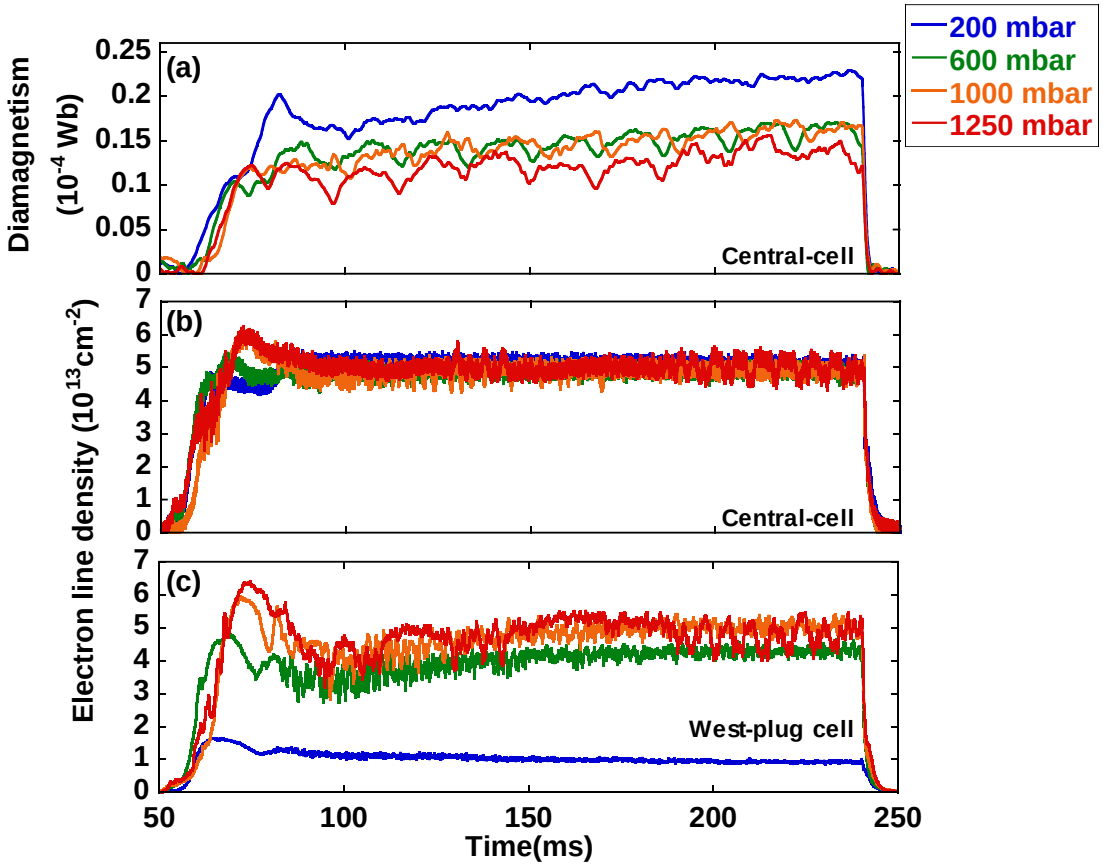

Fig.5.1 (a) Diamagnetism in the central-cell, (b) electron line density in the central-cell and (c) west-plug cell at each plenum pressure.

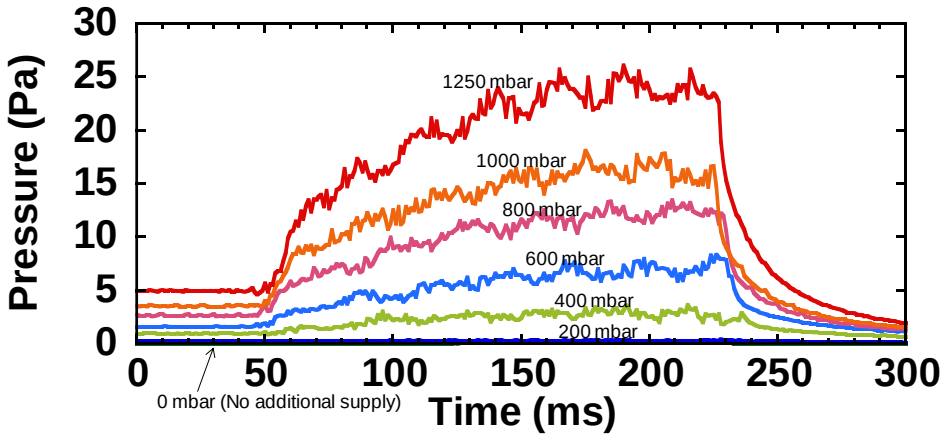

Fig.5.2 Time evolution of the hydrogen gas pressure in the D-module, which is measured with the ASDEX gauge at each plenum pressure.

5.2.2 Plasma parameters of detached plasma

Figure 5.2 shows the time evolution of the neutral gas pressure (P_{H2}) in the D-module in the case of each plenum pressure. The plasma was produced from 50 ms. The neutral gas pressure became constant before plasma discharge and increased from just after plasma discharge. It means that the outflow of gas from the D-module was suppressed by interactions of plasma and gas.

Figure 5.3 shows T_e, n_e and Balmer line intensities ($I_{H\alpha}$, $I_{H\beta}$, $I_{H\gamma}$ and $I_{H\delta}$) in D-module as a function of neutral gas pressure. The electron temperature measured with Langmuir probe of No. 3 decreased from about 25 eV to around 1 eV or less with the increase in P_{H2}. The electron density increased with the increase in P_{H2} up to around 1.5 Pa and then it decreased. It is indicating a density rollover and plasma detachment. Balmer-alpha intensity increased with the increase in P_{H2} up to around 8 Pa and then it decreased. The pressure dependence of $I_{H\beta}$, $I_{H\gamma}$ and $I_{H\delta}$ show the similar trend to the electron density up to P_{H2} ~ 12 Pa. The intensity of Balmer-β, Balmer-γ and Balmer-δ shows the sudden increase around at P_{H2} ~ 12 Pa, but Balmer-α

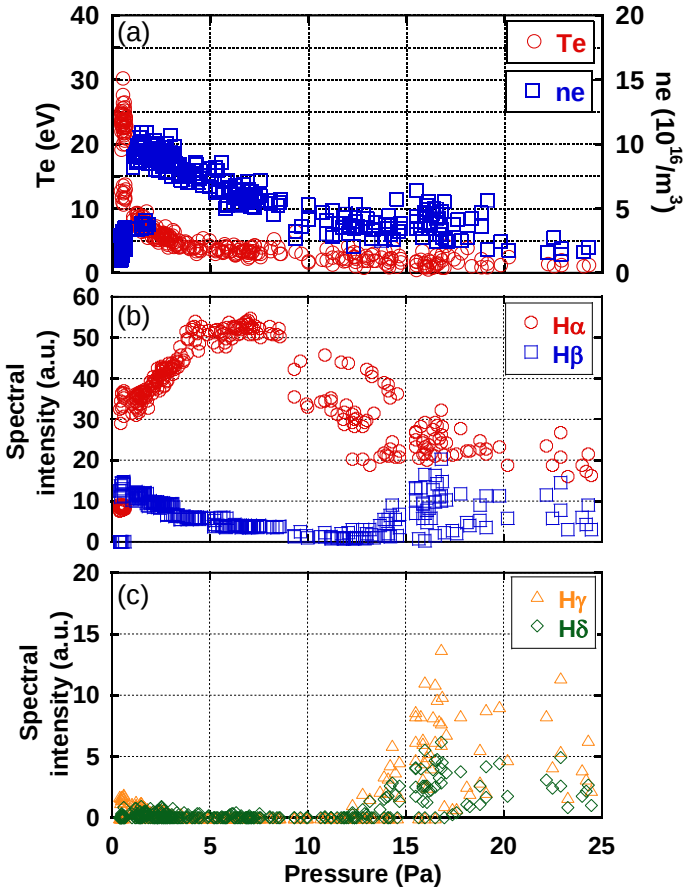

Fig.5.3 The electron temperature and electron density, (b) intensities of H_α and H_β emission, and (c) intensities of H_γ and H_δ emission measured by the spectroscopy (USB2000+) as a function of the hydrogen gas pressure.

intensity almost did not change as shown in Fig.4. At around P_{H2} ~ 12 Pa, the plasma condition changed from a state with the emission from mostly low excited hydrogen atoms to the state with significant emission from the highly excited hydrogen atom. This transition is hereinafter referred to as "High Excitation (HE) transition", and which will be discussed in later chapters.

5.2.3 Spatial distribution of MAR

Figure.5.4(a)-(h) shows two-dimensional of the Balmer-α and Balmer-β intensities in front of the V-shaped target in the case of each of plenum pressure. Intensities are averaged in the duration which plasma was steady state (i.e. t = 100ms ~ 160ms). Balmer-α intensity became stronger at the upstream side (i.e. left-hand side of the image) with increasing neutral gas pressure up to around 10Pa, and it decreased when the neutral gas pressure was around 12 Pa. On the other hand, Balmer-β intensity near the upstream side increased up to the neutral gas pressure of ~ 2 Pa and then decreased. The Balmer-α and Balmer-β intensities near the corner of the V-shaped target decreased significantly at the high neutral gas pressure, respectively. It means that the detached plasma was produced in front of the V-shaped target. The ratio of Balmer-α and Balmer-β intensities is a good indicator for the occurrence of MAR in the detached plasma. Figures 5.4(i)-(l) show the spatial distribution of the ratio of Balmer-α intensity to Balmer-β intensity ($I_{H\alpha}/I_{H\beta}$) at each plenum pressure. Figures 5.5 show the $I_{H\alpha}$, $I_{H\beta}$ a ratio of those intensities as a function of a distance along the central axis from the corner of the V-shaped target (i.e. z (mm)). The data of Fig. 5.6 are picked up from the data of distribution of Fig. 5.5. The unevenness of the intensity as shown at z ~ 130, 230 and 335 mm are caused by the reflection of the edge of the flange installed at the D-module. As the neutral gas pressure increased, the value of $I_{H\alpha}/I_{H\beta}$ increased and the region with a high ratio of $I_{H\alpha}/I_{H\beta}$ moved from the corner to the upstream side, thus indicating that the region with the significant occurrence of the MAR spread and moved from corner to the upstream side. As shown in Fig.5.6, the intensity ratio of $I_{H\alpha}/I_{H\beta}$ increased and the peak position of it moved to the upstream side with increasing the neutral gas pressure, respectively.

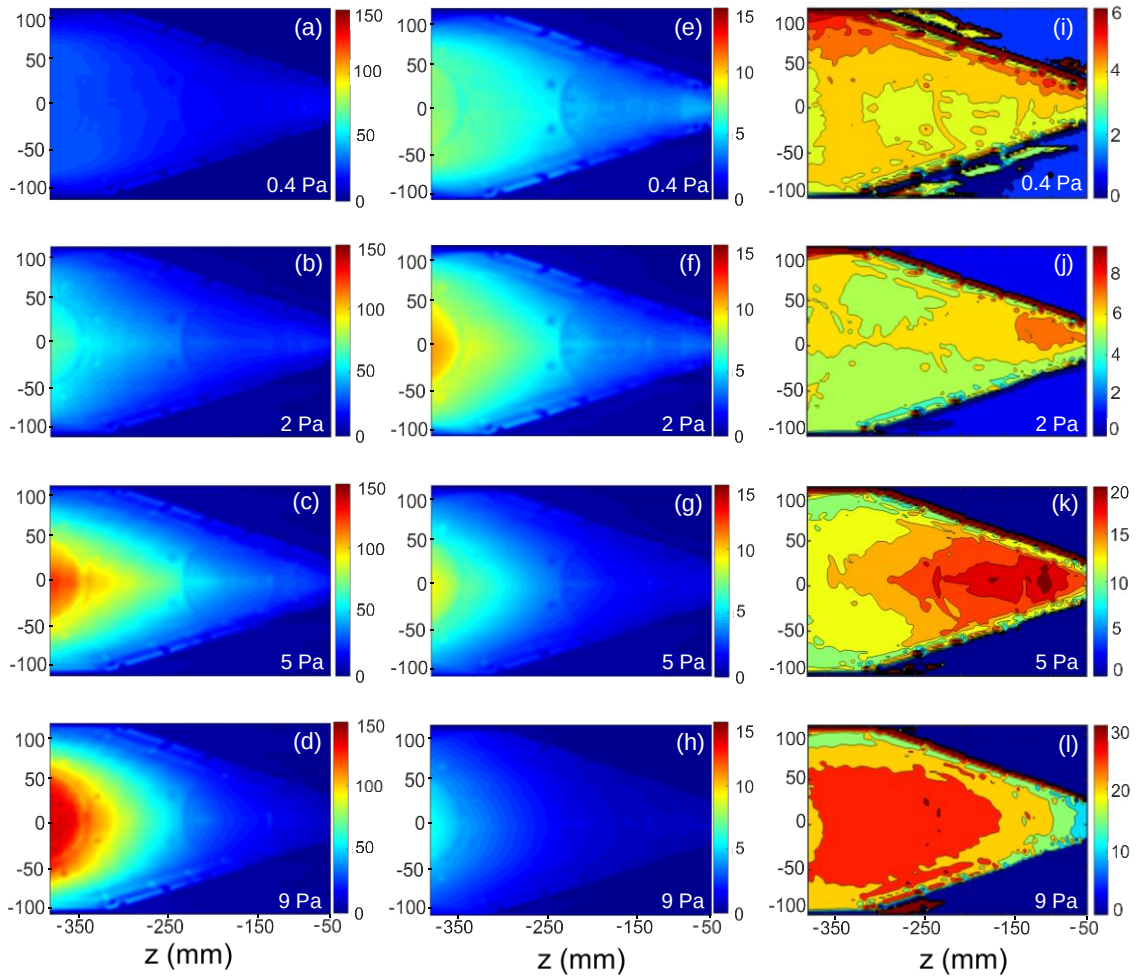

Fig.5.4 (a)-(d) Two dimensional images of H_α line intensity, (e)-(h) two dimensional images of H_β line intensity and (i)-(l) ratio of H_α intensity and H_β intensity ($I_{H\alpha}/I_{H\beta}$).

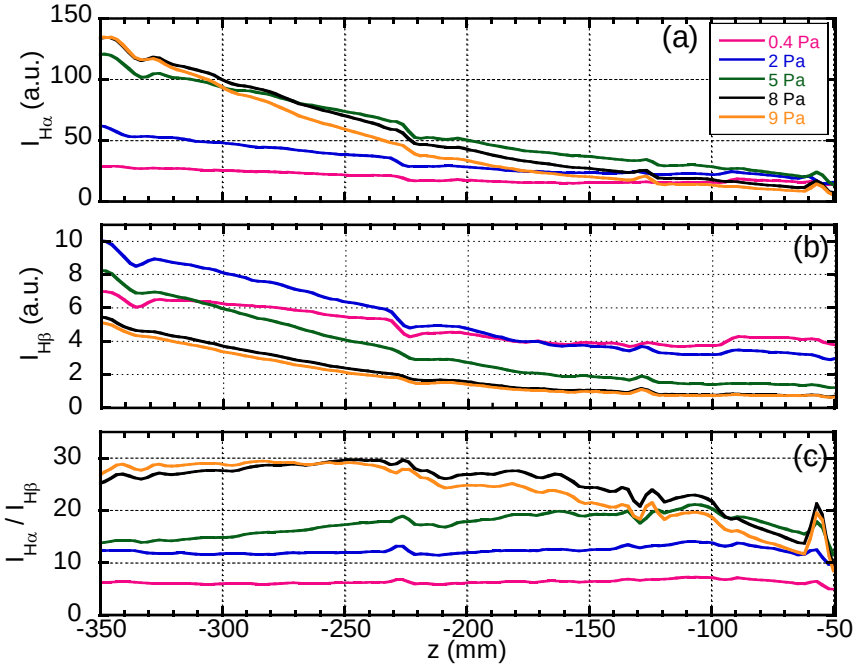

Fig.5.5 (a) H_α line intensity, (b) H_β line intensity and (c) ratio of the H_α line intensity to the H_β line intensity ($I_{H\alpha}/I_{H\beta}$).

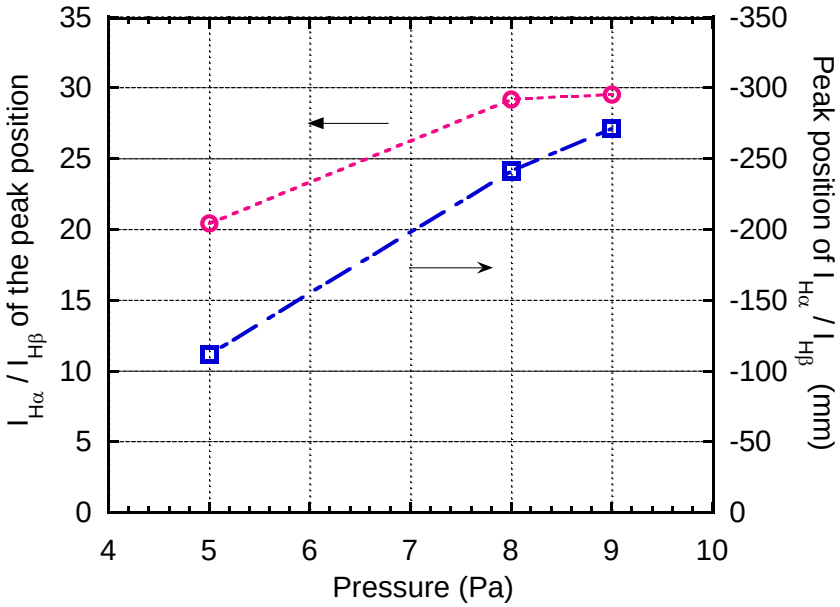

Fig.5.6 Pressure dependence of the peak position of $I_{H\alpha}/I_{H\beta}$ and $I_{H\alpha}/I_{H\beta}$ at the peak position.

5.2.4 Observation of transition to MAR with population inversion

Figure 5.7 shows the typical emission spectrum before and after the HE transition. The Balmer line emissions from highly excited atoms (H(n=11)) appeared after the HE transition, although the Balmer emissions from only the excited atoms with $n \leq 7$ were observed before the HE transition. Figure 5.8 shows the relative population density (n_n / g_n) before and after the HE transition. The value of n_n is obtained from Balmer line intensities shown in Fig. 5.7 divided by each Einstein coefficient. The number of atoms excited at n=3 did not change before and after the HE transition. Before the HE transition, the number of atoms excited more than n=3 decrease with the excitation energy. On the other hand, a population inversion with the value of n_H(n=5) larger than n_H(n=4) was clearly observed after the HE transition. Figure 5.9 shows the spatial distributions of the H_α and H_β line intensities measured with the high-speed camera before and after the HE transition. The spatial distribution of the H_β intensity changes drastically before and after the HE transition. A strong emission of the H_β was observed at the center of the plasma. The H_α line intensity decreases from the upstream toward the corner either before and after the HE transition.

Figure 5.10 shows the typical Fulcher-α band spectrum and the relative population density of $H_2(d^3\Pi_u^-)$ of twelve rovibrational states before the HE transition at $P_{H2} \sim 8$ Pa. In the case of Fig. 5.10(b), the assuming of the coronal model for states of $X^1\Sigma_g^+$, $d^3\Pi_u^-$ and $a^3\Sigma_g^+$ can estimate that the vibrational temperature of hydrogen molecules is around 10,000 K. Since the plasma density is low (i.e. $n_e < 10^{18}$ /m^3) in this experiment, the assumption of this coronal model is considered to be valid. As shown in Fig. 5.11(a), T_{vib} increased from around 4,000 K to around10,000 K with the increase in P_{H2} up to around 2 Pa and then decreased down to around 2,000K. As shown in Fig. 5.11(b), T_{rot} increased from around 500 K to around 1,400 K with the increase in P_{H2} up to around 5 Pa and then decreased down to around 1,000K.

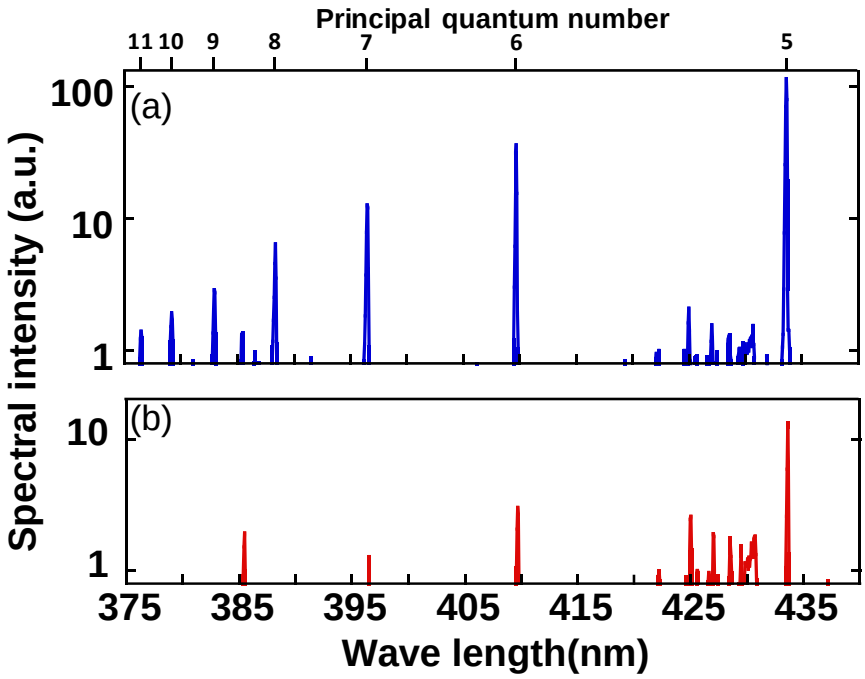

Fig. 5.7 The spectral intensity (a) before and (b) after the HE transition.

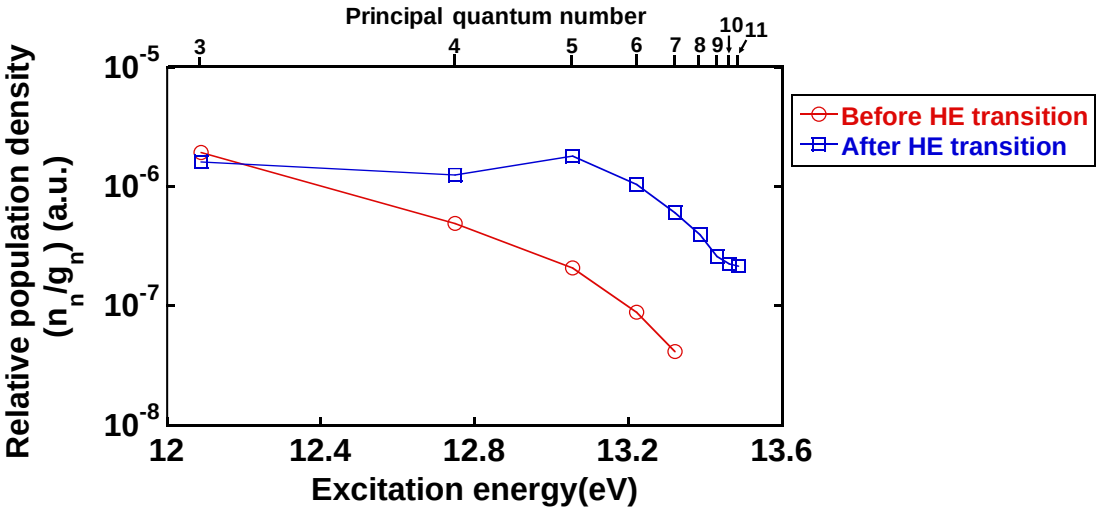

Fig.5.8 Relative population density as a function of the excitation energy. The lines are a guide to the eye.

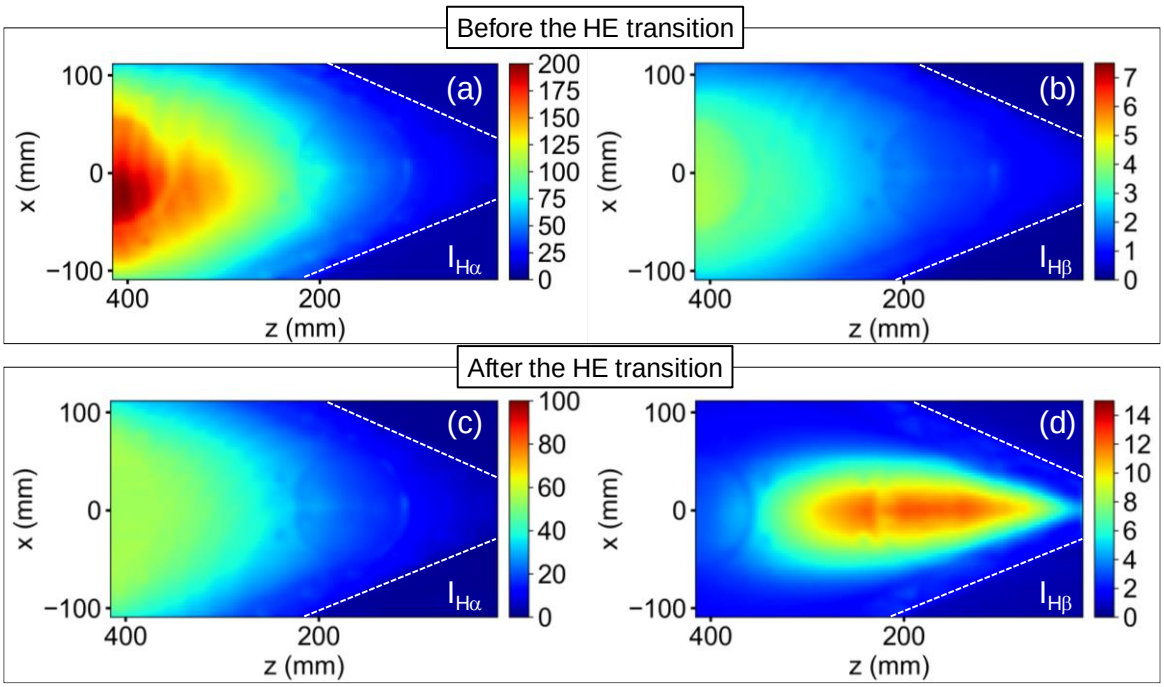

Fig.5.9 Images of Balmer line intensity in front of the V-shaped target measured by the fast camera attached with interference filter which has 656 nm and 486 nm of the center wavelength and 10 nm of half maximum full-width. (a) I_{Ha} at P_{H2} ~ 11 Pa, (b) I_{Hb} at P_{H2} ~ 11 Pa, (c) I_{Ha} at P_{H2} ~ 15 Pa, and (a) I_{Hb} at P_{H2} ~ 15 Pa. Note that white dash line indicates surface of V-shaped target.

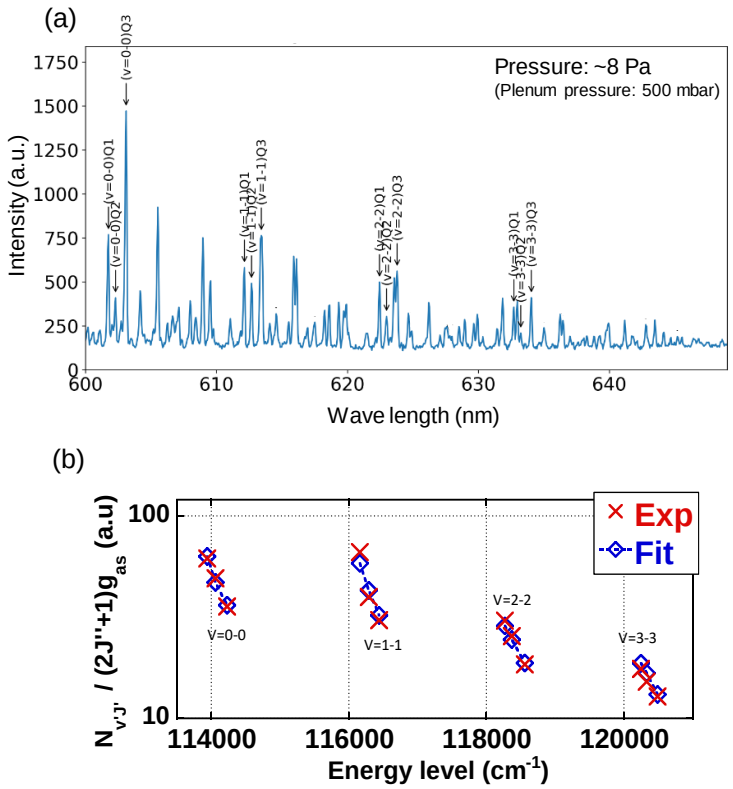

Fig.5.10 (a) Fulcher-α band spectrum and (b) relative population densities of $d_3\Pi_u^-$ for various rovibrational states at the hydrogen gas pressure of 8 Pa.

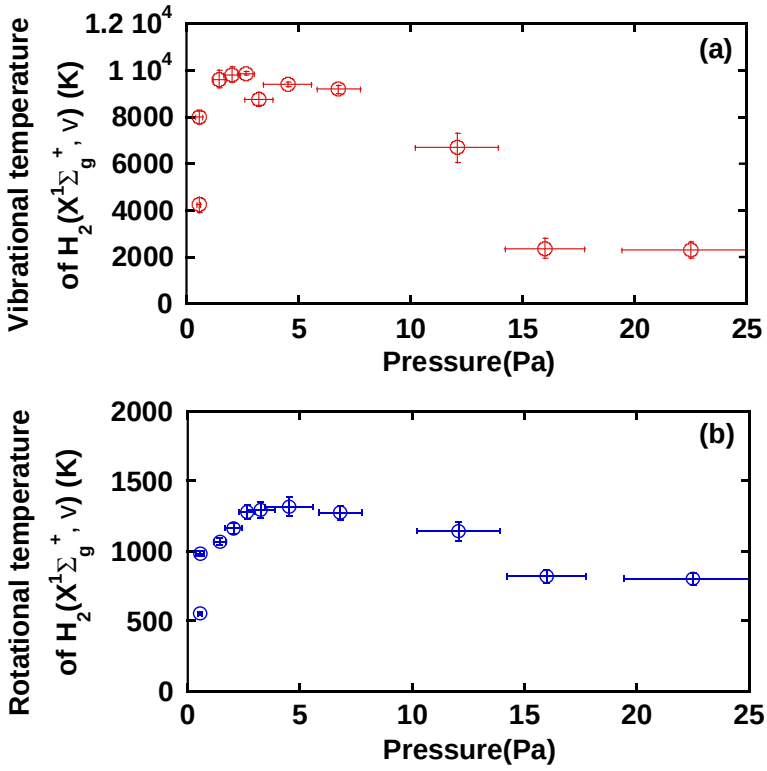

Fig.5.11 (a) Vibrational temperature and (b) rotational temperature as a function of the hydrogen gas pressure.

5.3 Discussion

5.3.1 Recombination processes of the detached plasma

It is revealed that the production mechanism of plasma detachment in the divertor simulation plasma is closely related with MAR processes associated with triatomic molecules [87]. The significant increase in $I_{H\alpha}$ during the plasma detachment as shown in Fig5.3, which should be caused mainly by the process of DA-MAR. The reaction chain of the DA-MAR process is promoted by the increasing the number of vibrationally excited molecules produced by the process of MIC-MAR. As shown in Fig. 5.11, the population density of vibrationally excited molecules are estimated from T_{vib} and P_{H2}. In Fig. 5.11, it is assumed that the vibrational excitation level (v) of n_{H2} follows Boltzmann-Maxwell distribution with T_{vib} and all of the hydrogen molecules are at the electronic ground state. Since T_{vib} is quite high (~ 10,000K) when P_{H2} is ~ 8 Pa, the value of $n_{H2(v)}$ is significantly larger in the case of P_{H2} ~ 8 Pa than in the case of P_{H2} ~ 1 Pa. It is revealed that the vibrationally molecules produced by the reaction of DR3 strongly contribute to the plasma detachment in the D-module, because of the value of $n_{H2(v)}$ at P_{H2} ~ 8 Pa is about two orders of magnitude larger than that at P_{H2} ~ 1 Pa.

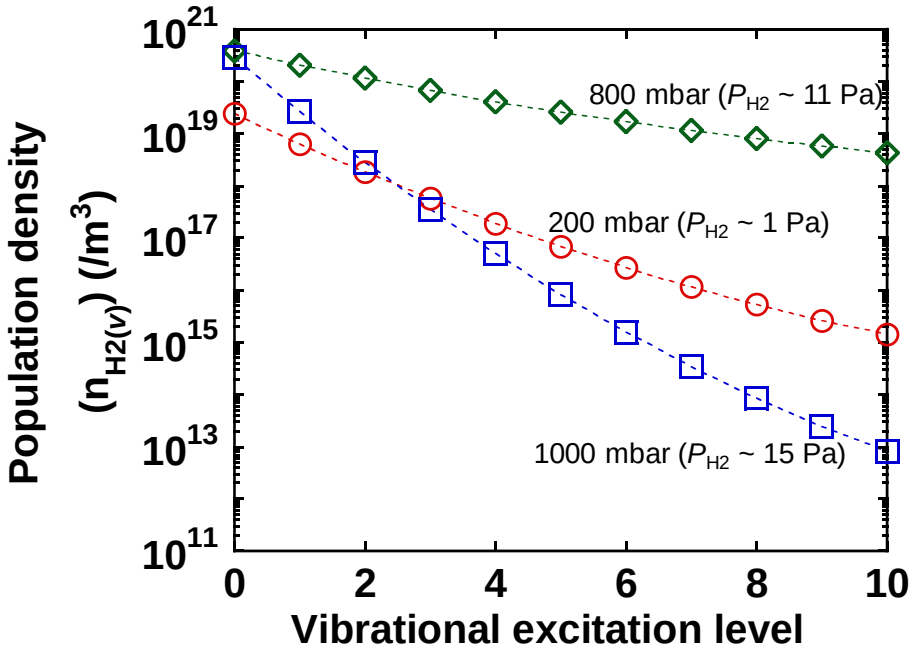

Fig.5.11 Population density of hydrogen molecule H2(X1Σg+, v) at each plenum pressure. The lines are a guide to the eye.

5.3.2 MAR with highly excited Balmer emissions and population inversion

As shown in Fig. 5.3, a sudden increase in $I_{H\beta}$, $I_{H\gamma}$ and $I_{H\delta}$, and population inversion were observed when P_{H2} is higher than 12 Pa. The formation of population inversion and production of highly excited atoms are caused by the three-body recombination in the recombination plasma [30]. However, since n_e is quite low and T_e ~ 1eV after the HE transition in this experiment, the three-body recombination could not occur in the D-module. A possible candidate for the formation of the population inversion is the following reaction hereinafter referred as MN2 [73].

$$H_2^+ + H^- \rightarrow H_2 + H(n \geq 2) \tag{5.1}$$

The population inversion similar to our experimental result is shown in the experimental results in the cascaded arc discharge plasma in Ref [88-90]. The cross-section of the MN2 reaction is the largest in the production of H(n=5). In our experiment, since the population density of vibrationally excited molecules is quite low as shown in Fig. 5.11, the number of H- produced by the DA reaction should become quite low after the HE transition. The reason for the decrease in $I_{H\alpha}$ would be suppressed the DA reaction due to the decrease in the number of H^-. As a process of H^- production involved with the MN2 reaction, a resonant ionization process [68, 69, 71] shown in the following reactions seems to be a strong candidate:

$$H(2s) + H(2s) \rightarrow H^+ + H^-(2l2l'), \tag{5.2}$$

$$H^+ + H^-(2l2l') \rightarrow H_2^{**}, \tag{5.3}$$

$$H_2^{**} \rightarrow H^+ + H^-. \tag{5.4}$$

The excited hydrogen atom of H(2s) react with each other, and H^- is produced through chain reactions in the resonant ionization process. The excited hydrogen atoms with n=2 are considered to be still produced by the IC-MAR process after the HE transition. H(n=2) produced by IC-MAR process seems to contribute the resonant ionization. The MIC-MAR leading to the DA-MAR processes are suppressed since T_{vib} becomes rather low after the HE transition, but the IC-MAR process is hardly affected by the decrease of T_{vib}.

5.4 Summary

The reaction processes of MAR leading to plasma detachment have been investigated in the divertor simulation experiments on GAMMA 10/PDX. The plasma was sustained by ion cyclotron heating, and the V-shaped target which was installed in the D-module was exposed to the end-loss plasma. Hydrogen gas was additional supplied to the D-module to produce detached plasma due to MAR.

The electron temperature decreased from ~ 15 eV to ~ 1 eV with increasing P_{H2}. On the other hand, ne increased with increasing P_{H2} up to ~1.5 Pa and then it decreased (i.e. so-called a density rollover), indicating the plasma detachment. The H_α line intensity continued to increase even though ne decreased after the density rollover. At that time, the intensity ratio $I_{H\alpha}/I_{H\beta}$ increased and the peak position of $I_{H\alpha}/I_{H\beta}$ moved to the upstream side and the area of high $I_{H\alpha}/I_{H\beta}$ spread. This indicates that MAR was enhanced with increase in the neutral gas pressure and the region of the MAR occurrence spread and moved to the upstream side, since $I_{H\alpha}/I_{H\beta}$ is a good monitor of MAR occurrence.

The vibrational temperature of hydrogen molecule increased up to ~10,000 K with increasing P_{H2}. The population density of the vibrationally excited molecules also significantly increased with increasing P_{H2}, which is attributed to production of vibrationally excited molecules that are produced by the DR3 reaction of the MIC-MAR process. This increase in the vibrationally excited molecules caused the continuous increase in the H_α intensity after the density rollover through the DA-MAR process.

Sudden increase in $I_{H\beta}$, $I_{H\gamma}$ and $I_{H\delta}$ and population inversion (i.e. the HE transition) has been observed when P_{H2} is higher than 12 Pa. The population inversion seems to be caused by the MN2 reaction because the cross section of H(n=5) production is the largest in the MN2 reaction. The negative ions for the MN2 reaction can be produced by resonant ionization process although the DA-MAR process, which produces the negative ions, becomes suppressed by decrease in T_{vib} after the HE transition. The excited hydrogen atoms with n=2, which are used in the resonant ionization process, can be still produced by the IC-MAR process after the HE transition, since the cross section of the IC-MAR process does not depend largely on T_{vib}.

Chapter 6
Dynamic behavior of plasma detachment caused by MAR

In this section, we will discuss the response of plasma detachment caused by MAR to plasma density modulation. The change of the spatial distribution of plasma detachment and the change of MAR due to transient particle flux will be also discussed.

6.1 Experimental method

The main plasma was produced and maintained from t = 50 ms to t = 250 ms by ICRF heating and gas puffing mainly in the central-cell of GAMMA 10/PDX. On the similar way as in section 5, hydrogen gas was supplied to the D-module from 300 ms before the plasma production until the end of plasma discharge. The ECH was applied in the central-cell in order to measure the dynamic response to the density modulation of divertor simulation plasma. The ECH was applied from 160 ms to 185 ms at 70 kW.

6.2 Experimental result and Discussion

Figure 6.1shows the time evolution of the electron line density and the diamagnetism at the central-cell when detached plasma is produced in the D-module (i.e. plenum pressure is 600 mbar). The ECH was applied from t = 160 ms to t = 185 ms. The electron line density and the diamagnetism increase during ECH. The electron temperature at central cell measured by Thomson scattering also increased from about 10 eV to about 47 eV due to ECH as shown in Fig. 6.2(b). The increase ratio of the electron line density is larger at the plug-cell than at the central-cell, which is considered to be affected that the gas supplied to the D-module.

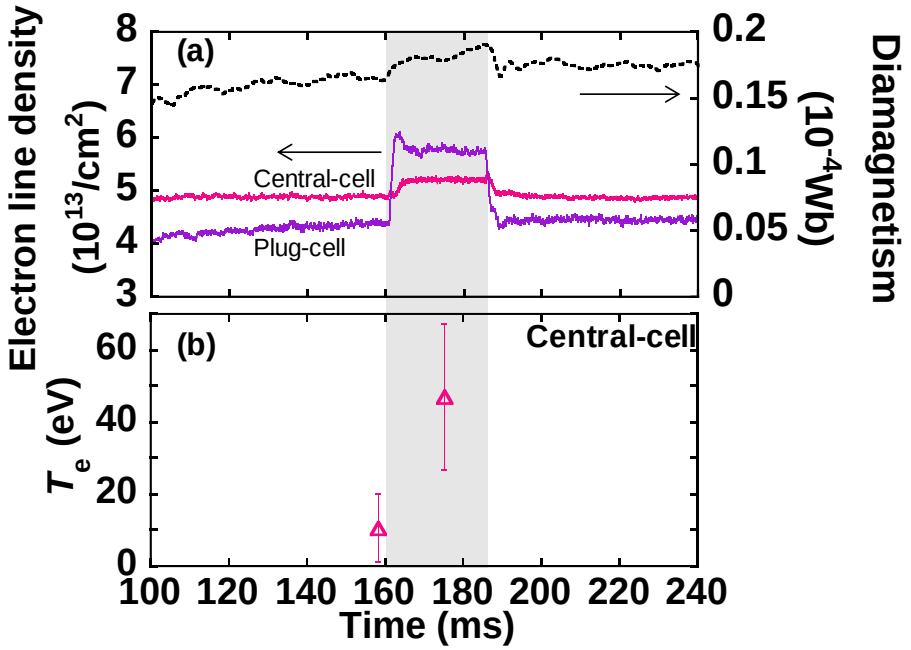

Fig.6.2 Time evolution of (a) the electron line densities at the central cell and plug cell plasmas, and diamagnetism of the central cell plasma, (b) the electron temperature of the central cell plasma.

Figure 6.2 shows electron line density at the plug-cell, T_e, n_e, $I_{H\alpha}$ and $I_{H\beta}$ in the D-module as a function of plenum pressure in the case of ECH applying and without ECH. The electron line density at the plug-cell increase with increasing plenum pressure. The electron line density with ECH is larger than that without ECH when plenum pressure more than 400 mbar. It means that ECH contributes to the increase in the particle flux flowing to the D-module when plenum pressure more than 400 mbar. As shown in Fig. 6.2 the electron temperature is not affected by ECH in the case of hydrogen gas is supplied. The value of T_e decreases to ~4 eV with the increase in the plenum pressure. The electron density increases with the increase in the plenum pressure until around 200 mbar and then it decreases (i.e. density rollover) in both case of with and without ECH. The decrease in T_e and density rollover indicates that the detached plasma was produced in the D-module. The increase in n_e by ECH is caused by ionization in the D-module when plenum pressure was 200 mbar. When plenum pressure is more than 400 mbar, ne in the D-module is increased due to ionization in the D-module and the increase in the particle flux flowing to the D-module. In both cases of with ECH and without ECH, the dependence of $I_{H\beta}$ on the plenum pressure is similar to that of n_e. On the other hand, $I_{H\alpha}$ continues to increase even though the electron density decreases with the increase in plenum

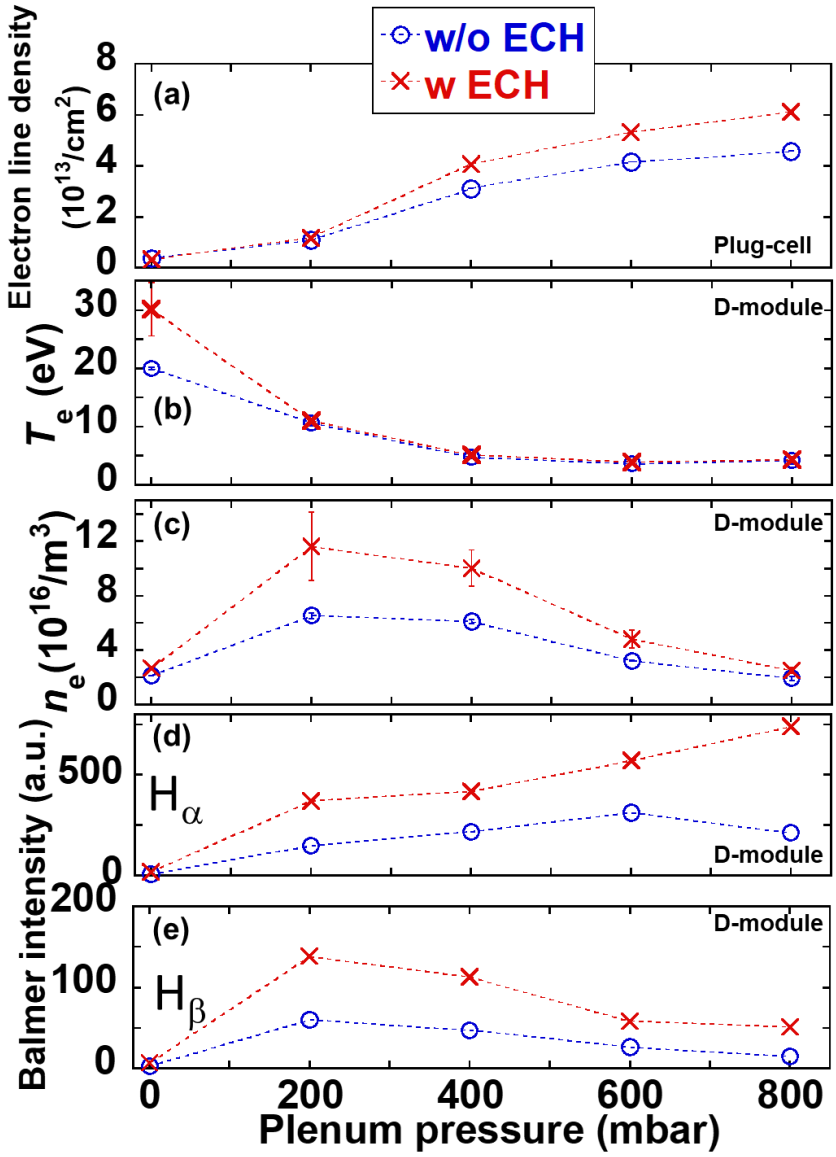

Fig.6.2(a) Electron line density at the plug cell, (a) electron temperature, (b) electron density, (c) Hα and (d) Hβ intensities in the D-module as a function of the plenum pressure. Electron temperature and electron density were measured by a Langmuir probe at the position of No.1 and Balmer intensity measured by spectroscopy (USB2000+). The dashed lines are a guide to the eye.

pressure until 800mbar in the case of without ECH. In the case of with ECH, $I_{H\alpha}$ increases with the increase in plenum pressure until 600 mbar, and then it decreases. The continuous increase in $I_{H\alpha}$ is caused mainly by the MAR associated with tri-atomic ion [91]. The decrease in $I_{H\alpha}$ at 800 mbar without ECH is considered to be attributed to the suppress of DA reaction associated with the decrease in vibrational temperature of molecules [91].

Figure 6.3 shows the time evolution of T_e and n_e on the surface of the V-shaped target during plasma detachment (i.e. plenum pressure is 600 mbar). The electron temperature measured

with a Langmuir probe of No.5 was decreased by ECH but T_e measured with probe No.1 and No.3 did not change. The electron density increased due to ECH and these increase ratios were about 1.5 ~ 2 times at each probe. The difference between ne measured with probe No.3 and No.5 is decreased by ECH, thus indicating that the spatial distribution of ne was changed. This observation means the ionization front moved from corner of the V-shaped target to the upstream side by ECH. The decreasing T_e at probe C should be involved in the movement of the ionization front to the upstream side. The electron temperatures at probe No.1 and No.3 were not affected by ECH. A possible explanation of this observation is that the plasma was already detached before ECH. This is consistent with that the ionization front moved to the upstream side by ECH. Therefore, in this experiment, the production of plasma detachment was proceeded by ECH.

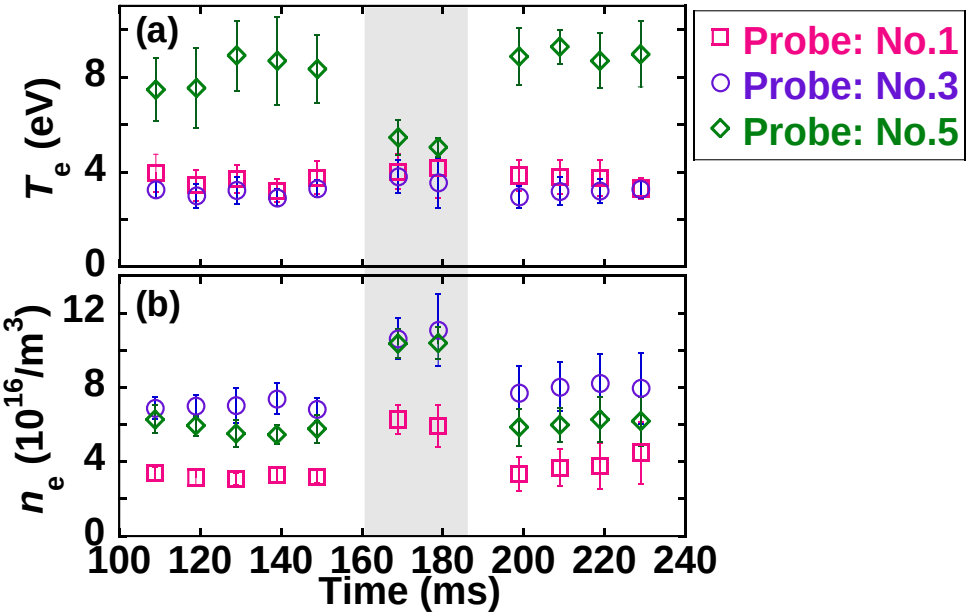

Fig.6.3 Time evolution of (a) the electron temperature and (b) the electron density on the V-shaped target.

Figure 6.4 shows the spatial distribution of $I_{H\alpha}$ and $I_{H\beta}$ with and without ECH during plasma detachment. The concentric ring structure near the corner of the V-shaped target (x~0 mm, z~80 mm) is the lens unit attached on quartz windows for Thomson scattering measurement. The data of Fig. 6.4 is averaged from t=150ms to t=160ms and from t=170ms to t=180ms, respectively. The values of $I_{H\alpha}$ and $I_{H\beta}$ decrease from the upstream side to the corner of the V-shaped target in both cases of ECH applying and without it, which indicates production of detached plasma. The values of $I_{H\alpha}$ and $I_{H\beta}$ in front of the V-shaped target are increased by ECH, respectively. The increase in $I_{H\alpha}$ and $I_{H\beta}$ is due to increasing ne in the D-module.

Figure 6.5 shows the time evolution of $I_{H\alpha}/I_{H\beta}$ near the corner of the V-shaped target (x = 0 mm, z = -40 mm) and in the upstream side (x = 0 mm, z = -170 mm). The position near the corner

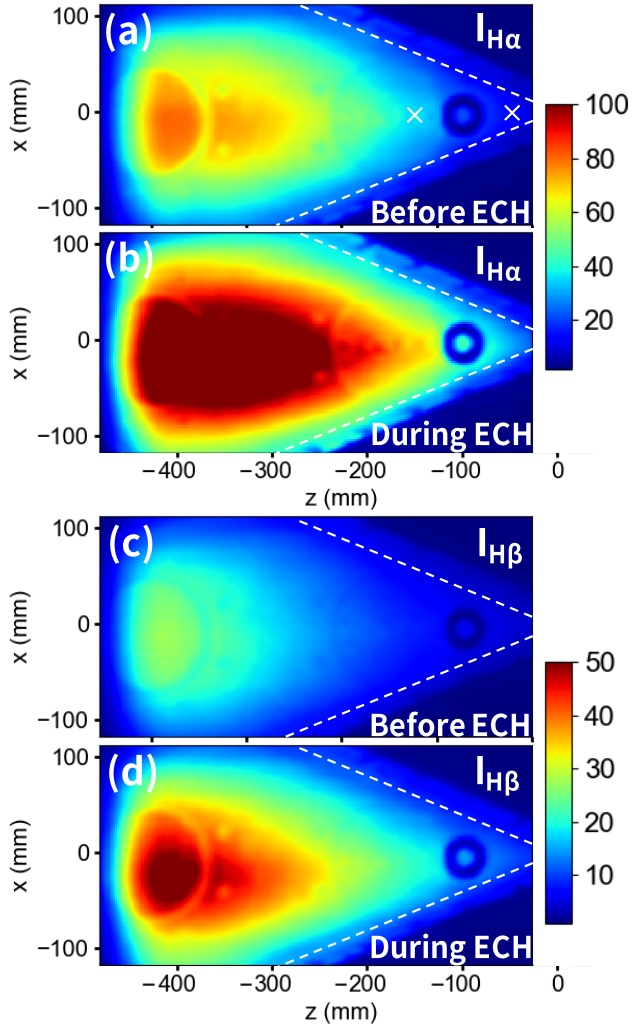

Fig.6.4 Two-dimensional images of Balmer line intensities in front of the V-shaped target measured by the high-speed camera. (a) $I_{H\alpha}$ before ECH and (b) $I_{H\beta}$ during ECH. (c) $I_{H\alpha}$ before ECH and (d) $I_{H\beta}$ during ECH. White dash lines indicate the surface of V-shaped target.

of the V-shaped target (x = 0 mm, z = -40 mm) and the upstream side (x = 0 mm, z = -170 mm) are hereinafter defined as view spot No.10 and No.9. The data of $I_{H\alpha}/I_{H\beta}$ in Fig. 6.5(a) are normalized by the values without ECH (i.e. normalized at 159 ms). The positions of the view spots of No.10 and No.9 are the same as that of SR500i shown in Fig. 4.7. The ratio of $I_{H\alpha}/I_{H\beta}$ can be used for a good indicator of the occurrence of MAR for the plasma detachment due to MAR. As shown in Fig. 6.5(a), the value of $I_{H\alpha}/I_{H\beta}$ at the view spot No.10 decreased just after ECH applying and then increased. On the other hand, the ratio at the view spot No.9 decreased by ECH applying. It is suggested that the occurrence of MAR in the view spot of No.10 increased, but it at No.9 decreases. The rapid decrease and increase in $I_{H\alpha}/I_{H\beta}$ just after ECH on and off is caused by slower change in $I_{H\alpha}$ than $I_{H\beta}$. The slow change seems to be caused by the change of MAR processes. Figure 6.5(b) shows the Q1-branch intensity of the Fulcher-α band (I_{Q1}), which is normalized by the value without ECH (i.e. at 132 ms). The value of I_{Q1} at view spot of No.10

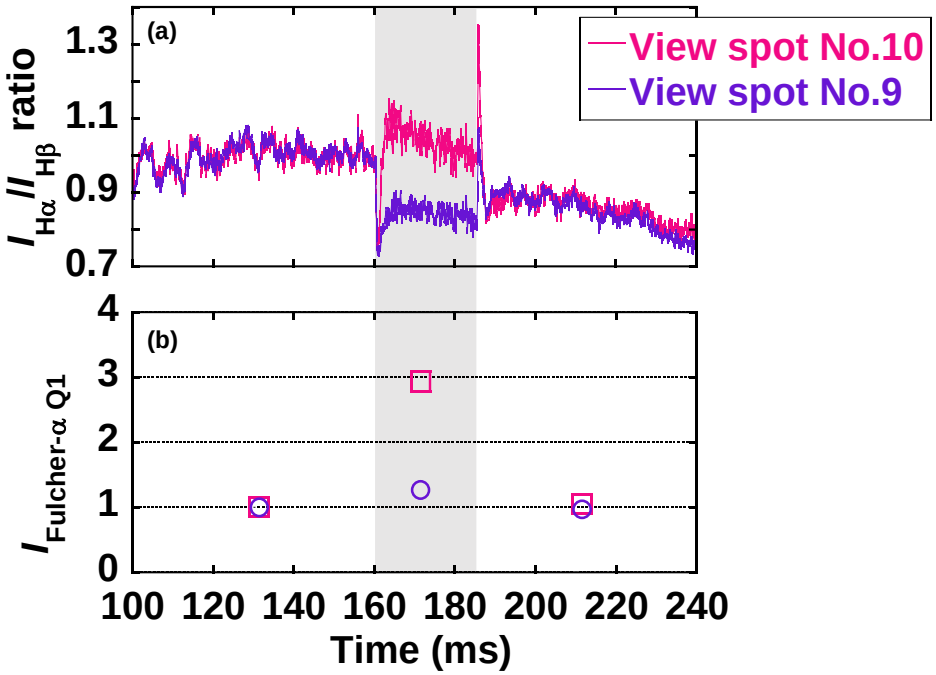

Fig.6.5 Time evolution of (a) $I_{H\alpha}/I_{H\beta}$ and (b) I_{Q1} at view spot of No.10 and No.9. Each value is normalized by the value of without ECH.

increases about three times by ECH although the increase in I_{Q1} at view spot of No.9 is about 1.3 times. The Q1-branch intensities are proportional to electron density, molecular density and the rate coefficient of electron-impact excitation shown as $H_2(X^1\Sigma_g^+) \rightarrow H_2(d^3\Pi_u^-)$. Q1-branch intensities are proportional to electron density, molecular density and the rate coefficient of electron-impact excitation shown as $H_2(X^1\Sigma_g^+) \rightarrow H_2(d^3\Pi_u^-)$. As a mentioned section 3.2.1, the rate coefficient depends greatly on the vibrational level of ground state molecule $(X^1\Sigma_g^+)$ as well as T_e. As shown in Fig. 6.5(b), the increase ratio of n_e by ECH was about 1.5 times, and the electron temperature in the D-module was not affected. In the D-module, the vibrational level of hydrogen molecules would not depend on the change in the particle flux due to ECH because the mean free path of electron-impact excitation has a large distance due to the plasma is low-density. Hence, the significant increase in I_{Q1} at No.10 by ECH seems to be attributed to the increase in the density of hydrogen molecules. This increase in the molecular density should be attributed to the increasing of hydrogen recycling flux near the corner of the V-shaped target due to the increase in the flux.

Figure 6.6(a) and 6.6(b) shows two-dimensional images of $I_{H\alpha}/I_{H\beta}$ in front of the V-shaped target before and during ECH. Before applying ECH, $I_{H\alpha}/I_{H\beta}$ is large at the target front (z ~ 150 mm). The value of $I_{H\alpha}/I_{H\beta}$ in front of the V-shaped target is smaller during ECH than before ECH. It means that MAR was suppressed by ECH in front of the V-shaped target. As shown in Fig. 6.6(b), $I_{H\alpha}/I_{H\beta}$ is smaller at the lower side than at the upper side. It indicates the deviation of the ECH. Figure 6.6(c) shows $I_{H\alpha}/I_{H\beta}$ during ECH normalized by $I_{H\alpha}/I_{H\beta}$ before ECH. In other

words, Figure 6.6(c) shows the change of the amount of MAR by ECH. In Fig 6.6(c), the values of $I_{H\alpha}/I_{H\beta}$ is large near the corner and surface of the target. It means that the increase in the amount of MAR by ECH was localized in the region close to the target.

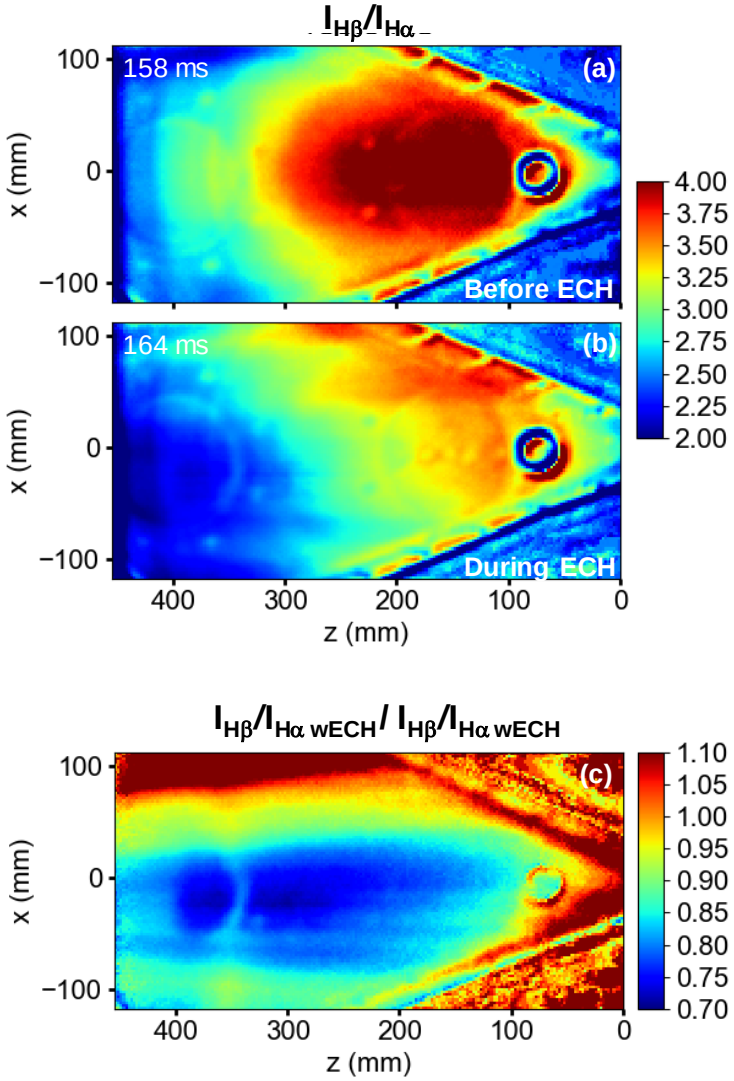

Fig.6.6 Two-dimensional images of $I_{H\alpha}/I_{H\beta}$ in front of the V-shaped target. (a) $I_{H\alpha}/I_{H\beta}$ before ECH and (b) $I_{H\alpha}/I_{H\beta}$ during ECH. (c) $I_{H\alpha}/I_{H\beta}$ during ECH normalized by $I_{H\alpha}/I_{H\beta}$ before ECH.

Figure 6.7 shows the spatial distribution of $I_{H\alpha}/I_{H\beta}$ on the z-axis. The data of Fig. 6.7 was extract from the data of Fig. 6.6. Consequently, the values of $I_{H\alpha}/I_{H\beta}$ in Fig. 6.7 has been normalized by the values without ECH (i.e. at 132 ms), and it means the change of the distribution shape of $I_{H\alpha}/I_{H\beta}$ by ECH as in Fig. 6.6. The value of $I_{H\alpha}/I_{H\beta}$ increase from the upstream side to the corner of the V-shaped target by ECH. In the region close to the corner of V-shaped target (i.e. -57 mm < z < -10 mm), $I_{H\alpha}/I_{H\beta}$ is larger than 1. It suggests that the occurrence of MAR enhanced close to the corner (-57 mm < z <- 10 mm) and it declined towards to the upstream side by ECH.

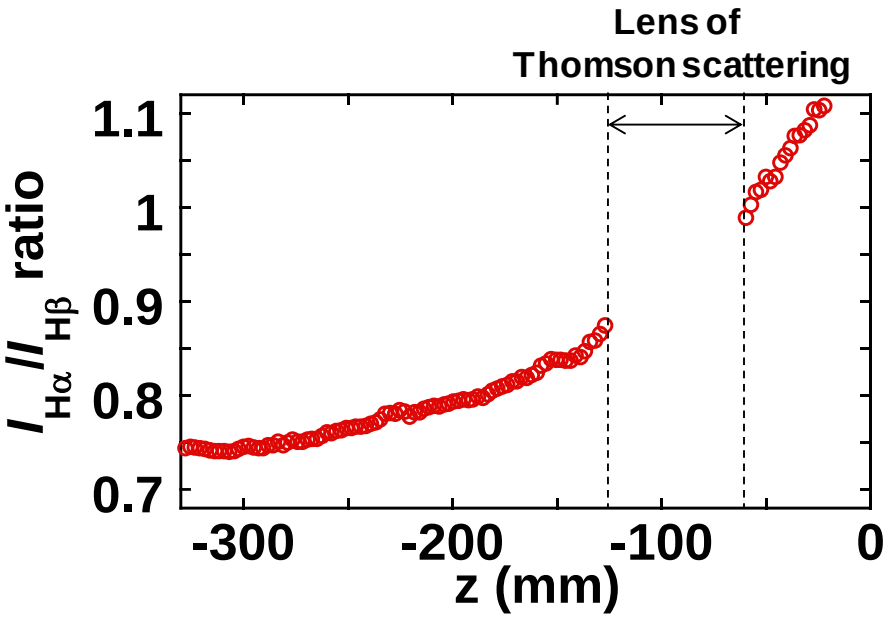

Fig.6.7 Spatial distribution of $I_{H\alpha}/I_{H\beta}$ ratio on the z-axis at t = 164 ms. It is normalized by the value of without ECH (t = 159 ms).

6.3 Summary

In this chapter, the response of plasma detachment caused by MAR to plasma density modulation was discussed. The density modulation of divertor simulation plasma was investigated by additional power injection utilizing ECH in the main plasma. In this experiment, hydrogen gas was supplied to the D-module to produce detached plasma due to MAR, and ECH was applied to the main plasma. In the case of additional gas supply, ne increased, but T_e was not affected by ECH. The ionization front moved to the upstream side due to ECH. The ratio of $I_{H\alpha}/I_{H\beta}$ near the corner of V-shaped (-57 mm < z < -10 mm) increased by ECH, thus indicating that the amount of MAR is increased near the corner. The increase in the amount of MAR by ECH was localized in the region close to the target due to the increase in the recycling flux. The increase in I_{Q1} near the corner of the V-shaped target by ECH indicates the increase in the density of hydrogen molecules by the increase of hydrogen recycling flux.

Chapter 7
Conclusion

In this study, experiments have been conducted utilizing end-loss plasma of GAMMA 10/PDX in order to clarify the behavior of hydrogen in the hydrogen recycling and plasma detachment caused by MAR.

Hydrogen recycling experiments using a high temperature tungsten target were performed to clarify the state of desorbed hydrogen molecules from the plasma-facing wall. Hydrogen molecules desorbed from the target were found to be in the vibrational excited state. In addition, it was revealed that the increase in Balmer line intensity by the increase in the target temperature is due to the increase in the number of vibrational excited hydrogen molecules desorbed from the target. This study revealed that the excited atoms increase due to the desorption of vibrational excited molecules from the plasma-facing wall, and its suggesting that the desorption of vibrational excited molecules contributes greatly to the density distribution of the edge plasma in tokamak devices.

In order to clarify the behavior of hydrogen in detached plasma caused by MAR, Experiments on the production of detached plasma by MAR in the diverter simulation plasma were conducted, and the atomic and molecular processes were discussed. It was revealed that the vibrational excited molecules produced by the DR3 reaction ($H_3^+ + e \rightarrow H_2(v) + H$) contributed to the change in the Ha intensity in the plasma detachment caused by MAR. In addition, it was found that the formation of population inversion in detached plasma by MAR is caused by MN2 reaction ($H_2^+ + H^- \rightarrow H_2 + H(n \geqq 2)$). Besides, it is suggested that negative ions contributing to MN2 reaction are produced by Resonant ionization process since the negative ion production by the DA reaction ($H_2(v) + e \rightarrow H^- + H$) is not dominant due to the number of vibrational excited molecules decrease. In order to clarify response of plasma detachment caused by MAR to plasma density modulation, additional ECH was applied to the main plasma of GAMMA 10/PDX during plasma detached in the D-module. It was found that, density of hydrogen molecules increased near the surface of the V-shaped target due to an increase in the inflowing flux, and the amount of production of MAR was increased. In addition, it was revealed that the increase in the occurance of MAR due to the increase of flux was localized near the surface of target.

Those findings and understandings gained from this study will contribute to further understanding of the physics in the edge-plasma, and the understanding of the atomic-molecular process of MAR for exploring possibilities of MAR in the detached diverter.

Acknowledgements

First of all, the author would like to express his greatest appreciation to Prof. Mizuki Sakamoto at University of Tsukuba for his generous support, elaborated guidance, and considerable encouragement in the course of the present study. His guidance helped me in all the time of research and writing of this thesis. I could not have imagined having a better advisor and mentor for my Ph.D study. Without his help, the present study would not have been possible.

I would like to deeply appreciate Prof. Keiji Sawada at Shinshu University and Dr. Shinichiro Kado at Kyoto University for their significant discussions and invaluable aids and suggestions for the investigating the atomic and molecular processes.

I would particularly like to thank to Prof. Yousuke Nakashima at University of Tsukuba for their advice, comment and continuing interest in the present study.

I especially thanks to Dr. Naomichi Ezumi at University of Tsukuba and Tsuyoshi Kariya at University of Tsukuba for their insightful comments and encouragement but also for the hard question which incented me to widen my research from various perspectives.

I would like to deeply appreciate Dr. Takaaki Iijima, Dr. Satoshi Togo, Dr. Md. Shahinul Islam, Dr. Kensuke Oki and Dr. Kazuya Ichimura for helpful advices.

I wish to express his appreciation to Mr. Kunpei Nojiri and Mr. Shuhei Sumida for their helpful discussions, advises and encouragements.

I also wish to thanks to members of BP group in Plasma research center for their discussions and encouragements.

I would like to thank the members of plasma research center for their collaboration in the experiments and for helpful discussion.

This study is partly supported by the bi-directional collaboration research program of National Institute for Fusion Science and University of Tsukuba.

Finally, I wish to thank my parents for their love, encouragement, supporting me emotionally and financially.

References

[1] Energy Balances of OECD Countries online data service 2015 edition - (expires 30 April 2016).

[2] J.D. Lawson, et al., Proc. Phys. Soc. Sect. B. 70 (1957) 6–10.

[3] JET Team, Nucl. Fusion. 32 (1992) 187–203.

[4] S. Ishida, et al., Phys. Rev. Lett. 79 (1997) 3917–3921.

[5] Agreement on the Establishment of the ITER International Fusion Energy Organization for the Joint Implementation of the ITER Project, INFCIRC/702, IAEA, (2007).

[6] R. Hiwatari, et al., J. Plasma Fusion Res. 81 (2005) 903–916.

[7] L. Spitzer, Phys. Fluids. 1 (1958) 253.

[8] L.A. Artsimovich, et al., JETP Lett. 1 (1972) 72.

[9] F. Wagner, et al., Phys. Rev. Lett. 49 (1982) 1408–1412.

[10] K. McCormick, et al., J. Nucl. Mater. 266–269 (1999) 99–108.

[11] G. Janeschitz, et al., J. Nucl. Mater. 220–222 (1995) 73–88.

[12] P. Stangeby, Nucl. Fusion. 33 (1993) 1695–1705.

[13] G.F. Matthews, J. Nucl. Mater. 220–222 (1995) 104–116.

[14] S. Takamura, et al., Nucl. Fusion. 28 (1988) 183–191.

[15] T. Shoji, et al., J. Nucl. Mater. 176–177 (1990) 830–836.

[16] K. Okano, et al, Fusion Res. 1 (1986) 413.

[17] S.A. Self and H.N. Ewald, Phys. Fluids. 9 (1966) 2486.

[18] A. Loarte, et al., Nucl. Fusion. 38 (1998) 331–371.

[19] P.H. Rebut, et al, Fusion Eng. Des. 22 (1993) 7–18.

[20] L. Schmitz, et al., Phys. Plasmas. 2 (1995) 3081–3094.

[21] N. Ohno, et al., J. Nucl. Mater. 220–222 (1995) 279–283.

[22] ITER Physics Basis Editors, Nucl. Fusion 39 (1999) 2137.

[23] M.E. Perry, et al., Nucl. Fusion. 31 (1991) 1859–1875.

[24] T. Eich, et al., Nucl. Mater. Energy. 12 (2017) 84–90.

[25] D. Tskhakaya, et al., Contrib. to Plasma Phys. 48 (2008) 89–93.

[26] P. Lang, et al., Nucl. Fusion. 44 (2004) 665–677.

[27] J. Kim, et al., Nucl. Fusion. 52 (2012) 114011.

[28] S. Takamura, et al., Plasma Sources Sci. Technol. 11 (2002) A42–A48.

[29] A. Loarte, et al., Nucl. Fusion. 38 (1998) 331–371.

[30] N. Ohno, et al., Nucl. Fusion. 41 (2001) 1055–1065.

[31] T. Iijima, et al., Plasma Fusion Res. 9 (2014) 2405010–2405010.

[32] M.L. Watkins, et al., Plasma Phys. Control. Fusion. 36 (1994) B241–B251.

[33] W.L. Hsu, et al., Phys. Rev. Lett. 49 (1982) 1001–1004.

[34] F. Scotti, et al., J. Nucl. Mater. 390–391 (2009) 303–306.

[35] R.K. Janev, et al., J. Nucl. Mater. 121 (1984) 10–16.

[36] D.E. Post, J. Nucl. Mater. 220–222 (1995) 143–157.

[37] P.S. Krstic, et al., J. Phys. B At. Mol. Opt. Phys. 32 (1999) 3485–3509.
[38] P.S. Krstic, et al., J. Phys. B At. Mol. Opt. Phys. 32 (1999) 2415–2431.
[39] R.C. Isler, et al., Phys. Plasmas. 4 (1998) 2989.
[40] D. Lumma, at el., Phys. Plasmas. 4 (1998) 2555.
[41] U. Wenzel, at el., Nucl. Fusion. 39 (1999) 873–882.
[42] V.A. Soukhanovskii, at el., Nucl. Fusion. 49 (2009) 095025.
[43] S.I. Krasheninnikov, at el., Phys. Lett. A. 214 (1996) 285–291.
[44] M.A. Lieberman, et al., Principles of plasma discharges and materials processing, John Wiley & Sons (2005).
[45] N. Ohno, et al., Phys. Rev. Lett. 81 (1998) 818–821.
[46] A. Tonegawa, at el., J. Nucl. Mater. 313–316 (2003) 1046–1051.
[47] E.M. Hollmann, at el., Rev. Sci. Instrum. 72 (2001) 623–626.
[48] J.L. Terry, at el., Phys. Plasmas. 5 (1998) 1759–1766.
[49] U. Fantz, at el., J. Nucl. Mater. 290–293 (2001) 367–373.
[50] D. Mihalas, at el., Astrophys. Space Sci. 8 (1970) 50–52.
[51] D.M. Mattox, Handbook of physical vapor deposition (PVD) processing, William Andrew (2010).
[52] M. Schaffer, at el., Nucl. Fusion. 36 (1996) 495–501.
[53] H. Takenaga, at el., Nucl. Fusion. 41 (2001) 1777–1787.
[54] M. Kobayashi, at el., J. Nucl. Mater. 350 (2006) 40–46.
[55] J. Jacquinot, at el., Plasma Phys. Control. Fusion. 35 (1993) A35–A52.
[56] R. Maingi, at el., Nucl. Fusion. 36 (1996) 245–253.
[57] H. Takenaga, at el., J. Nucl. Mater. 337–339 (2005) 802–807.
[58] R. Kumazawa, at el., Nucl. Fusion. 46 (2006) S13–S21.
[59] M. Sakamoto, at el., Nucl. Fusion. 44 (2004) 693–698.
[60] Equipe Tore Supra (prepared by F. Saint-Laurent), Nucl. Fusion. 40 (2000) 1047–1055.
[61] J. Harris, at el., Surf. Sci. 105 (1981) L281–L287.
[62] Y. Nakashima, at el., Nucl. Fusion. 57 (2017) 116033.
[63] T.E. Sharp, At. Data Nucl. Data Tables. 2 (1970) 119–169.
[64] F. Jensen, Introduction to computational chemistry, John wiley & sons, 2017.
[65] R. Sanderson, Chemical bonds and bonds energy, Elsevier, 2012.
[66] H.M. Crosswhite, The hydrogen molecule wavelength tables of Gerhard Heinrich Dieke, Wiley-Interscience, 1972.
[67] R.K. Janev, at el., Collision processes in low-temperature hydrogen plasmas, Forschungszentrum Jülich, Zentralbibliothek 2003.
[68] J. Komppula, at el., AIP Conf. Proc. 1515 (2013) 66–73.
[69] J.S. Vogel, Rev. Sci. Instrum. 87 (2016) 02A503.
[70] M. Bacal, M. Wada, Appl. Phys. Rev. 2 (2015) 021305.
[71] J.S. Vogel, AIP Conf. Proc. 1655 (2015) 020015.
[72] T. Mosbach, Plasma Sources Sci. Technol. 14 (2005) 610–622.
[73] M.J.J. Eerden, at el., Phys. Rev. A. 51 (1995) 3362–3365.

[74] I. Kovács, at el., Acta Phys. Hungarica. 54 (1983) 161–187.
[75] B. Xiao, at el., Plasma Phys. Control. Fusion. 46 (2004) 653–668.
[76] U. Fantz, Plasma Sources Sci. Technol. 15 (2006) S137–S147.
[77] M. Capitelli, at el., Formation of Vibrationally and Rotationally Excited Molecules During Atom Recombination at Surfaces, Springer New York (2016) 57–78.
[78] C. Schermann, at el., J. Chem. Phys. 101 (1994) 8152–8158.
[79] N. Ezumi, at el., J. Nucl. Mater. 266–269 (1999) 337–342.
[80] S. Kajita, at el., J. Nucl. Mater. 313–316 (2003) 748–753.
[81] S. Kajita, at el., Contrib. to Plasma Phys. 44 (2004) 607–612.
[82] M. Inutake, at el., Phys. Rev. Lett. 55 (1985) 939–942.
[83] K. Oki, at el., Fusion Sci. Technol. 68 (2015) 81–86.
[84] K. Ichimura, at el., Rev. Sci. Instrum. 87 (2016) 11D424.
[85] S. Markelj, at el., J. Chem. Phys. 134 (2011) 124707.
[86] S. Kado, at el., J. Nucl. Mater. 337–339 (2005) 166–170.
[87] M. Sakamoto, at el., Nucl. Mater. Energy. 12 (2017) 1004–1009.
[88] O. Gabriel, at el., AIP Conf. Proc. 1097 (2009) 22–30.
[89] W.E.N. Van Harskamp, at el., Phys. Rev. E. 83 (2011) 036412.
[90] W.E.N. Van Harskamp, at el., Plasma Sources Sci. Technol. 21 (2012) 024009.
[91] A. Terakado, et al., 23nd International Conference on Plasma Surface Interactions in Controlled Fusion Devices, submitted to Journal of nuclear materials and energy.